Title

Abnormal development of auditory responses in the inferior colliculus of a mouse model of Fragile X Syndrome

Journal

Journal of Neurophysiology, 123(6)

ISSN

0022-3077

Authors

Nguyen, Anna O
Binder, Devin K
Ethell, Iryna M
et al.

Publication Date

2020-06-01

DOI

10.1152/jn.00706.2019

Peer reviewed

Abnormal development of auditory responses in the inferior colliculus of a mouse model of Fragile X Syndrome

Anna Nguyen[1], Devin K. Binder[2,3], Iryna M. Ethell[2,3], Khaleel A. Razak[2,4]*

[1]Bioengineering Program, [2]Graduate Neuroscience Program, [3]Division of Biomedical Sciences and [4]Psychology Department, University of California, Riverside, United States

*Corresponding Author:
Khaleel A. Razak, PhD
Department of Psychology
Email: Khaleel@ucr.edu
Phone: 951-827-5060

Running Title: Correlates of auditory hypersensitivity in FXS

Number of Figures: 12
Number of Tables: 6

Keywords: Fragile X Syndrome, Autism, sensory processing disorder, midbrain, seizures, auditory processing, development

We report no conflict of interest.

Acknowledgements: This work was supported by the US Army Medical Research grant W81XWH-15-1-0436. We thank members of Drs. Ethell, Razak, and Binder laboratories for helpful discussions, comments, and technical support.

Key words: Fragile X Syndrome, autism, inferior colliculus, development, sensory hypersensitivity, seizures

Abstract

Sensory processing abnormalities are frequently associated with autism spectrum disorders, but the underlying mechanisms are unclear. Here we studied auditory processing in a mouse model of Fragile X Syndrome (FXS), a leading known genetic cause of autism and intellectual disability. Both humans with FXS and the *Fragile X mental retardation gene* (*Fmr1*) knock-out (KO) mouse model show auditory hypersensitivity, with the latter showing a strong propensity for audiogenic seizures (AGS) early in development. Because midbrain abnormalities cause AGS, we investigated whether the inferior colliculus (IC) of the *Fmr1* KO mice shows abnormal auditory processing compared to wild-type (WT) controls at specific developmental time points. Using antibodies against neural activity marker c-Fos, we found increased density of c-Fos+ neurons in the IC, but not auditory cortex, of *Fmr1* KO mice at P21 and P34 following sound presentation. *In vivo* single-unit recordings showed that IC neurons of *Fmr1* KO mice are hyper-responsive to tone bursts and amplitude-modulated tones during development, and show broader frequency tuning curves. There were no differences in rate-level responses or phase locking to amplitude-modulated tones in IC neurons between genotypes. Taken together, these data provide evidence for the development of auditory hyper-responsiveness in the IC of *Fmr1* KO mice. Although most human and mouse work in autism and sensory processing has centered on the forebrain, our new findings, along with recent work on the lower brainstem, suggest that abnormal subcortical responses may underlie auditory hypersensitivity in autism spectrum disorders.

New and Noteworthy

Autism spectrum disorders (ASD) are commonly associated with sensory sensitivity issues, but the underlying mechanisms are unclear. This study presents novel evidence for neural correlates of auditory hypersensitivity in the developing inferior colliculus (IC) in the *Fmr1* KO mouse, a mouse model of Fragile X Syndrome (FXS), a leading genetic cause of ASD. Responses begin to show genotype differences between postnatal days 14 and 21, suggesting an early developmental treatment window.

Introduction

Fragile X Syndrome (FXS) is a leading genetic cause of intellectual disability and autism that affects approximately 1 in 4000 males and 1 in 8000 females. An expansion of CGG repeats in the 5' un-translated region of the *Fragile X mental retardation 1* (*Fmr1*) *gene* causes its silencing and a loss of Fragile X Mental Retardation Protein (FMRP). FMRP is an RNA binding protein involved in translation regulation. The resulting abnormal protein synthesis in the brain during development leads to symptoms of FXS that include cognitive, anxiety and social deficits, hyperactivity, language impairments, increased susceptibility to seizures, and sensory impairments (Smith et al., 2012). A consistent and debilitating symptom of FXS is abnormal sensory reactivity (Rais et al., 2018), particularly hypersensitivity to sensory stimuli (Hitoglou et al., 2010; Rogers et al., 2003). Hypersensitivity manifests strongly in the auditory domain, but the underlying mechanisms are only begin to be elucidated (Ethridge et al., 2016; Garcia-Pino et al., 2017; Wang et al., 2017).

An animal model of FXS, the *Fmr1* knock-out (KO) mouse, displays several core FXS-like phenotypes including hyperactivity, social abnormalities, electrophysiological, and dendritic spine deficits (Bakker and Oostra, 2003; Kazdoba et al., 2014). Importantly, the *Fmr1* KO mouse also shows auditory hypersensitivity, including enhanced cortical responses to sounds, increased propensity for AGS and abnormal sensorimotor gating (Chen and Toth, 2001; Frankland et al., 2004; Rotschafer and Razak, 2013; Wen et al., 2018; Kokash et al., 2019). Electroencephalographic (EEG) recordings demonstrate remarkably similar phenotypes in the *Fmr1* KO mouse and humans with FXS (Castrén et al., 2003; Ethridge et al., 2017; Lovelace et al., 2016, 2018; Schneider et al., 2013). These include increased amplitude and reduced habituation of sound-evoked responses, increased resting gamma power and reduced consistency in phase locking to amplitude-modulated sounds. *In vivo* single unit and EEG recordings from the auditory cortex of *Fmr1* KO mice show abnormally increased responses to sounds during development and in adults (Rotschafer and Razak, 2013; Wen et al., 2018, 2019; Kulinich et al., 2020).

FMRP is expressed at multiple levels of the auditory system, and deficits in auditory processing are reported in the lower brainstem of the *Fmr1* KO mice (Beebe et al., 2014; Garcia-Pino et al., 2017; Rotschafer and Cramer, 2017; Rotschafer et al., 2015; Wang et al., 2014). A recent study showed that selective deletion of *Fmr1* from forebrain excitatory neurons only partially recapitulates cortical EEG phenotypes, and showed that increased resting state low (30-60 Hz), but not high (70-100 Hz), gamma power reported in global *Fmr1* KO is present in the forebrain specific knockout (Lovelace et al., 2019). These studies suggest that at least some of the abnormal responses recorded in the cortex are generated sub-cortically.

Audiogenic seizure (AGS) is a robust and consistently reported phenotype in the *Fmr1* KO mice, particularly between postnatal day (P)20 and P30 (Dölen et al., 2007; Michalon et al., 2012; Musumeci et al., 2007; Pacey et al., 2009; Yan et al., 2005). Multiple studies have suggested that abnormalities of the midbrain inferior and superior colliculi (IC, SC) underlie specific patterns of sensitivity and behaviors associated with AGS (Millan et al., 1986; Faingold and Randall, 1999; Faingold, 2002). Indeed, Gonzalez et al. (2019) showed that AGSs are induced by *Fmr1* deletion in VGlut2 expressing excitatory neurons in the inferior colliculus (IC). We recently found elevated levels of matrix metalloproteinase-9 in the developing IC of *Fmr1* KO mice compared to WT mice and deficits in pre-pulse inhibition of acoustic startle in *Fmr1* KO mice (Kokash et al., 2019), further suggesting early developmental deficits in IC. These studies suggest that responses IC neurons of *Fmr1* KO mice are abnormal during development and may underlie auditory hypersensitivity. The main goal of this study was to test this hypothesis and to identify developmental changes in IC responses to sound in *Fmr1* KO mice.

We used two different methods to quantify IC auditory responses in WT and *Fmr1* KO mice. The first aim was to use immunostaining for c-Fos to determine the number of activated cells in the IC, auditory thalamus, and auditory cortex at P21 and P34. We found a significantly higher number of activated cells in the IC of the *Fmr1* KO compared to WT mice. Second, we performed *in vivo* single unit recordings from IC at P14, P21 and P34 to determine minimum thresholds, response magnitudes, frequency tuning, and responses to amplitude-modulated tones. We report significant genotype differences of IC responses that correlate with the development of auditory hyper-responsiveness in *Fmr1* KO mice.

Methods

Animals

All animal procedures were approved by the University of California, Riverside Institution Animal Care and Use Committee. Breeding pairs of FVB.129P2−Fmr1tm1Cgr/*J (Fmr1* KO) and their congenic controls (WT) mice were obtained from Jackson Laboratories and bred in-house. All mice were housed in a 12:12 light/dark cycle and given standard lab chow and water *ad libitum*. Immunostaining against c-Fos was done on the brain slices of P21-22 WT (n=16), P34-39 WT (n=23), P21-22 *Fmr1* KO (n=15) and P34-39 *Fmr1* KO (n=23) mice. Single-unit electrophysiological recordings were obtained from the IC of P14-15 WT (n=9), P21-22 WT (n=11), P34-39 WT (n=12), P14-15 *Fmr1* KO (n=10), P21-22 *Fmr1* KO (n=10), and P34-39 *Fmr1* KO (n=9) mice. These groups will be referred to as P14, P21 and P34 mice below. Male mice were used for all experiments.

Sound exposure paradigm

Our goal was to examine the levels of neural activity marker c-Fos in the auditory pathway of *Fmr1* KO mice in response to relatively loud sounds, but without any overt motor behaviors associated with AGS. AGS behaviors include wild running and jumping and tonic seizure episodes that may lead to death (Dansie et al., 2013; Gonzalez et al., 2019). *Fmr1* KO mice, but not WT mice, are prone to AGS. Therefore, if the sound causes seizures, the associated motor responses involved would only be present in the KO mice and render the two groups incomparable in terms of sensory responses. Therefore,

149 we performed pilot tests to identify the highest sound level that does not cause any motor
150 responses associated with AGSs. These pilot data showed that the AGS threshold for P34
151 *Fmr1* KO mice was >90 dB SPL so we used 80 or 90 dB for 15 minutes (5-50 kHz
152 bandwidth, 500 ms upward modulated frequency sweep followed by 500 ms downward
153 modulated frequency sweep). However, 90 dB sounds induced AGSs in the P21 group, so
154 we used 85 dB SPL in this age group with 1000 ms of quiet in between each 1000 ms of
155 sound. Based on off-line video analysis, none of the mice used showed any motor
156 behaviors associated with AGSs. Therefore, there was no exclusion of mice to account
157 for motor behaviors. To perform c-Fos immunostaining, up to 4 male mice in the P21 or
158 P34 group were placed in a standard mouse cage with no food or water. Mice used for
159 immunohistochemistry of c-Fos were habituated for 3 h in a sound attenuated booth
160 (Gretch-Ken Inc.) before stimulus presentation. This would facilitate isolation of c-Fos
161 expression to the stimulus and minimize background c-Fos expression. In addition, these
162 mice remained in the sound attenuation booth for 45 min after offset of the sound
163 stimulus and before transcardial perfusion. Control groups underwent the same procedure
164 except no sounds were presented. Auditory stimuli were generated using custom software
165 (BATLAB, Dr. Don Gans, Kent State University or Sparkle, Portfors Lab, Washington
166 State University) and delivered through a programmable attenuator (PA5, TDT) and a
167 speaker (FT17H, Fostex International) placed face down on top of the cage lid. Sound
168 levels were measured with a sound level meter (735, B&K Precision) at a distance from
169 the speaker to the cage bottom. A lamp was used to provide light for a video camera to
170 record behaviors during 5 min of baseline with no sound presentation and 15 min of
171 sound presentation.

Immunohistochemistry

We examined the IC, the auditory thalamus, and core auditory cortex to determine if there are regional differences in c-Fos expression across genotypes. Two age groups of mice were used for the analysis of c-Fos+ cell density: P21 and P34. Mice were euthanized with sodium pentobarbital (Fatal-Plus, i.p. 125 mg/kg) for perfusion. Transcardial perfusion was done with cold 0.1 M PBS (pH=7.4) followed by cold 4% PFA (pH=7.6). The brain tissues were extracted and post-fixed overnight in 4% PFA before storage in 0.1 M PBS at 4^{o}C until further tissue processing in the future. The brains were cryoprotected in 30% sucrose for 2 days before being sectioned (CM 1860, Leica Biosystems) in the coronal plane at 40 µm thickness. All immunohistochemistry steps were done on a shaker at room temperature unless otherwise noted. For each mouse, two slices for each region of interest (IC, medial geniculate body, and auditory cortex) were used for c-Fos immunohistochemistry. Slices were chosen at ~50% in the rostrocaudal extent of the IC and MGB based on the Allen mouse brain atlas. This allowed for consistency in slice locations across mice. The shape of these nuclei also vary across the rostrocaudal extent, facilitating selection of comparable sections across mice. Consistency across mice in selecting the auditory cortex sections was based on the location of the dentate gyrus of the hippocampus. We have previously validated this method in Martin del Campo et al., (2012). Slices were washed 3x5 min in 0.1 M PBS followed by blocking with 5% Normal Goat Serum for 1 h. Slices were then washed with PBS for 10 min followed by 0.5% triton X-100 for 10 min. Next, the slices were incubated overnight in 4°C in primary rabbit anti-c-Fos antibody (1:100; SC-52, Santa

195 Cruz, RRID:AB_2106783) in 1% NGS and 0.1% Tween-20 in 0.1 M PBS. This antibody
196 is commonly used in mouse studies (e.g., Howorth et al., 2009; Numa et al., 2019),
197 including in studies of the central auditory system (Fulop et al., 2019). On the next day,
198 the slices were washed 3x5 min with PBS and incubated in secondary antibody (1:500;
199 donkey anti-rabbit Alexa 594) with 1% NGS and 0.1% Tween 20 in PBS for 2 h. Then,
200 the slices were washed in PBS 3x5 min and mounted on a glass slide with a mounting
201 medium (Vectashield H-1200, Vector Laboratories) and the edges were sealed (Cytoseal
202 60, Richard-Allan Scientific). The slides were stored in the dark at 4°C until imaging was
203 done. Stained sections were imaged using a confocal microscope (SP5, Leica
204 Microsystems) with 10x objective and a stack of 20 optical images was collected with
205 1024x1024 resolutions at 2µm z-steps. Image analysis was performed using ImageJ
206 Software (NIH). Because the MGB is composed of multiple divisions with different
207 functions, we evaluated c-Fos positive cell density in each division separately using Allen
208 Brain Atlas. The dimensions of the windows used for the cell counting in the different
209 divisions of the MGB are provided in Table 1. The sizes of these windows were selected
210 based on sufficient coverage of the divisions of interest across all photomicrographs. A
211 400 µm wide window that was at 45° angle to the midline of a coronal section was used
212 as the counting window for the IC (Figure 1A, B). Large images were stitched as needed
213 using the 'stitch' plugin (Preibisch et al., 2009) for ImageJ to obtain high resolution
214 images for counting. A rolling ball background subtraction was done for all images
215 (rolling ball radius = 6.6 µm) facilitating a removal of smooth continuous backgrounds.
216 c-Fos+ cell counts were based on intensity auto-thresholding of the pixels (Geometric
217 Triangle Function) and size (greater than 13.2 μm^2) in ImageJ for all images. The

Geometric Triangle Function is an auto-thresholding feature of ImageJ. This allows consistent thresholding parameters to be applied to all images, thus ensuring uniform thresholding across slices. The triangle algorithm draws a line 'b' from the maximum peak to the lowest value in an image's histogram. An orthogonal line 'd' is computed from line 'b' to the maximal distance of the histogram. A bin is formed from line 'd' to the maximum pixel intensity value. Then, all pixels in the image are converted to binary values (pixels within the bin as determined by the triangle algorithm and pixels not within the bin). Clusters of pixels that is greater than 20 px^2 (13.2 μm^2) are counted as c-Fos+ cells.

In vivo electrophysiology recordings from IC

In vivo extracellular single unit recordings were conducted in urethane (1 g/kg) and xylazine (20 mg/kg) (i.p. injection) anesthetized mice. Supplemental doses of anesthesia were given during recording sessions, as needed. A craniotomy was performed using a micro drill (Foredom Electric Co.) with coordinates based on skull landmarks. The IC was identified based on the transverse sinus vein, auditory responses, tonotopy, and post-hoc histology from Fluoro-Ruby dye injected in the recording site. A negative feedback rectal thermometer was used to maintain the temperature of the mice at 38 ±1 °C throughout the recording session. A calibrated speaker was placed contralateral to the recorded IC at a 45° angle and 6 cm away from the ear. A glass electrode (1 M NaCl, 2-10 MΩ impedance) was advanced using a micromanipulator (Kopf 2660) to depths between 200-2000 μm in the IC. Sound stimulation and data acquisition were driven by SPARKLE software (Sparkle Data Acquisition, Portfors Lab). Single units were isolated

and identified based on amplitude and constancy of spikes. Unless otherwise noted, each stimulus was repeated 20 times with a 2 Hz repetition rate. The stimulus duration was 50 ms including a 2 ms rise/fall time. The recording window used was 250 ms from stimulus onset except for the sinusoidal amplitude modulated (SAM) tones, in which the recording window was 1000 ms. Post stimulus time histogram data were analyzed offline. The number of neurons recorded from each group were: n=78 from P14-15 WT, n=77 from P21-22 WT and n=102 from P34-39 WT; n=81 from P14-15 *Fmr1* KO, n=84 from P21-22 *Fmr1* KO and n=83 from P34-39 *Fmr1* KO mice. Upon isolation of a neuron, spontaneous activity and response selectivity were quantified as described below.

Spontaneous activity and frequency response area

Spontaneous activity was recorded within the 250 ms recording window in the absence of any stimuli. The number of action potentials in the recording window was sampled over 20 repetitions (with no sound, 2 Hz repetition rate). Frequency tuning curves were constructed by measuring responses to tones with frequencies between 4 and 48 kHz in 4 kHz steps, and sound levels between 10 and 90 dB SPL in 10 dB steps. Each frequency/sound level combination was presented 20 times with a 2 Hz repetition rate. Characteristic frequency (CF) was defined as the frequency to which the neuron responded at the lowest sound level tested. Bandwidth (BW)10, BW20, and BW30 was the range of frequencies to which the neuron responded at 10 dB, 20 dB, and 30 dB above minimum threshold, respectively.

Rate-level functions

We determined the rate-level function of each neuron to quantify the changes in response magnitude with increasing sound levels. The CF tone was presented at levels between 10 and 90 dB SPL in a pseudo-random manner. The number of action potentials over 20 repetitions of each sound level was counted to plot the rate-level function. Percent turnover (%TO) and dynamic range were calculated from the rate-level functions as defined by (Phillips and Kelly, 1989). %TO was taken as $\%\,TO = \frac{\text{Max Response} - \text{Response to 90 dB SPL}}{\text{Max Response}} \times 100$. The higher the value of %TO, the more non-monotonic is the relationship between sound level and response magnitude and indicates that the response increases and then decreases as sound levels increase. A low %TO indicates either that the response increases continuously with sound level or that it saturates. We hypothesized that the *Fmr1* KO IC neurons would show reduced %TO compared to WT IC neurons. The dynamic range is the range of sound levels over which the response increases from 10% to 90% of maximum response. Across the population, the dynamic range is indicative of how rapidly the IC gets activated with increasing sound levels. We hypothesized that the *Fmr1* KO IC neurons would show narrower dynamic range compared to WT IC neurons.

Response magnitude and first spike latency

The average number of spikes per stimulus and the median first spike latency was calculated from the response of neurons to 20 repetitions (2 Hz rate) of CF tones presented at 15 dB and 30 dB above minimum threshold.

Selectivity for sinusoidal amplitude modulated sounds

Sinusoidal amplitude modulated (SAM) tones were used to determine temporal properties of IC neurons. The carrier frequency was at CF presented 15 dB above minimum threshold (500 ms duration and 2 ms rise/fall time). The recording window was 1000 msec in duration. The carrier tone was 100% depth modulated at the following frequencies: 5, 10, 20, 50, 100, and 200 Hz. Rate modulation transfer function (rMTF) was defined as the number of spikes per stimulus presentation for the duration of the stimulus presentation (500 msec). Temporal modulation transfer function (tMTF) was quantified as the vector strength (VS, Goldberg and Brown, 1969). Each spike time was correlated to the period phase (0-360 degrees). The VS was determined at each modulation frequency (5, 10, 20, 50, 100, and 200 Hz). In the tMTF period analysis, the first 100 ms of the recording duration was not included to omit the onset response to the sound stimulus (Liang et al., 2002; Overton and Recanzone, 2016).

Statistical Analysis

For the c-Fos analysis, the average of cell counts from 2 slices per brain region per animal was used with animal number as sample size. Mice were separated into quiet and sound-exposed groups. The P21 mice received one sound level (85 dB) and the P34 groups received one of two sound levels (80 or 90 dB). If the counts of c-Fos+ cells within a brain region showed normal distribution, then a Student's t-test was used for genotype comparisons. If any dataset within a brain region was not normally distributed, then all genotype comparisons within that brain region used the nonparametric Mann-Whitney U test. Genotype differences were analyzed by comparing the means of *Fmr1* KO vs WT separately for P21 and P34 groups. For the electrophysiology data a two-way

ANOVA with age and genotype as factors was performed to test main effects and interactions. The number of neurons was used as sample size for electrophysiology data. Unless otherwise noted, P value <0.05 was considered significant for ANOVA, Student's t-test and Mann-Whitney U test.

Results

Density of c-Fos+ cells was higher in the IC of *Fmr1* KO compared to WT mice at P21 and P34

The first major aim of the study was to determine potential genotype and age-dependent differences in the number of c-Fos+ activated cells in the IC, MGB, and auditory cortex. The density of c-Fos+ cells was counted in the quiet and sound-exposed conditions in P21 and P34 mice of both genotypes, corresponding to high and low AGS susceptible ages, respectively (Musumeci et al., 2000). After habituation for 3 h in a sound-attenuated booth, a siren-like sound (alternating 5-50 kHz upsweep for 500 msec and 50-5 kHz downsweep for 500 msec) was played for 15 min. Following perfusion, images of c-Fos immunoreactive labeling were collected and a 400 um-wide window, drawn diagonally in the dorsolateral to ventromedial direction of the IC, was selected for cell counting (Fig. 1 A-D). This window was further subdivided into two halves for analysis covering 0-50% and 51-100% of the IC in the dorsolateral to ventromedial direction.

In the quiet condition, a Student's t-test showed no significant genotype difference in the 0-50% region of the IC at P21 ($t(11)=-1.186$, $p=0.261$) or P34 (Figure 1E, $t(12)=0.841$, $p=0.417$). In the 51-100% region (Figure 1G), there was also no

significant genotype difference at P21. However, at P34 the density of c-Fos+ cells was significantly lower in the 51-100% region of the IC *Fmr1* KO mice compared to WT mice ($t(12)=3.618$, $p=0.004$). Thus, for ambient sound levels, the density of c-Fos+ cells in the IC was not higher in the *Fmr1* KO mice compared to WT mice at either P21 or P34.

However, when sounds were presented, the *Fmr1* KO mouse IC showed higher c-Fos+ cell density than WT group at both P21 and P34. Only a single sound level (85 dB) was tested for the P21 group so the data was analyzed using a Student's *t*-test. At P34,we tested mice at either 80 or 90 dB SPL and used a two-way ANOVA (sound level and genotype as factors) for the c-Fos+ cell density analysis. At P21, there was a significant increase in the sound-evoked c-Fos+ cell density in the 0-50% IC window of *Fmr1* KO mice compared to WT mice (Figure 1F, $t(16)=-2.907$, $p=0.010$). Interestingly, for the P34 group, there was a significant decrease in the density of c-Fos+ cells in the 0-50% IC window of *Fmr1* KO mice compared to the WT mice ($F(1,27)=5.415$, $p=0.028$).

In the more ventromedial (51-100%) half of the IC (Figure 1H), there was no significant difference at P21 between WT and *Fmr1* KO mice ($t(16)=-1.444$, $p=0.168$). At P34, c-Fos+ cell density was significantly higher in *Fmr1* KO mice compared to WT mice ($F(1,27)=5.216$, $p=0.030$). There was also a main effect of sound level with significantly higher c-Fos+ cell density at 90 dB compared to 80 dB sound level ($F(1,27)=4.998$, $p=0.034$). There was no genotype x sound interaction ($F(1,27)=1.734$, $p=0.199$) at P34. Thus, when exposed to sound, c-Fos+ cell density was higher in the IC of the *Fmr1* KO than WT mice, suggesting auditory hyper-responsiveness in the IC at both P21 and P34. The region of the IC showing increased c-Fos+ cell density in the

Fmr1 KO mice shifts with age (P21→P34) from more dorsolateral IC to more ventromedial locations.

Division specific genotype differences in c-Fos+ cell density in the medial geniculate body

The MGB is comprised of multiple divisions, including the medial (MGm), the ventral (MGv), the dorsal (MGd) divisions, and the suprageniculate nucleus (SGN) (Fig. 2). The adjacent peripeduncular nucleus (PP) may also be involved in auditory processing through reciprocal connections with the IC (Arnault and Roger, 1987). For the quiet condition data, a Mann-Whitney U test was used for genotype comparison in each MGB division. At P21, there was a significant increase in c-Fos+ cell density in *Fmr1* KO mice compared to WT mice in the MGm (U=5, p=0.014). There was no significant difference in other divisions of the MGB at P21 (PP (U=20, p=0.604), MGv (U=3.5, p=0.543), MGd (U=18, p=0.420), SGN (U=14.5, p=0.217). At P34, there was a significant increase in c-Fos+ cell density in *Fmr1* KO, compared to WT, mice in the MGv (U=8, p=0.01), but not in the other divisions (PP (U=26, p=0.574), MGd (U=15.5, p=0.083), MGm (U=17, p=0.106), SGN (U=28.5, p=0.712)).

In the sound-exposure condition, at P21, there was a significant increase in c-Fos+ cell density in the SGN (U=7.5, p=0.003) and PP (U=19, p=0.05) of the *Fmr1* KO mice compared to the WT. All other divisions showed no significant differences (MGv (U=38.5, p=0.858), MGd (U=22, p=0.102), MGm (U=20, p=0.069)). At P34, no genotype differences were present in any MGB division for sounds presented at 80 dB SPL: PP (U=17.5, p=0.370), MGv (U=17.5, p=0.368), MGd (U=13.5, p=0.158), MGm

(U=24, p=0.949) and SGN (U=20, p=0.565). When sound was at 90 dB, only the PP (U=29, p=0.05) showed a genotype difference. There were no differences in the other divisions (MGv (U=33, p=0.083), MGd (U=43, p=0.283), MGm (U=30.5, p=0.061) and SGN (U=54, p=0.760)). Thus, for ambient sound conditions, *Fmr1* KO mice show increased number of c-Fos+ activated cells in the MGm and MGv. When sound was presented, the SGN and PP showed higher number of c-Fos+ cells in *Fmr1* KO mice.

Auditory cortex does not show increased c-Fos+ cell density in *Fmr1* KO mice

Single unit recordings from auditory cortex (Wen et al., 2018) showed higher response magnitude in P21 *Fmr1* KO mice compared to WT mice, suggesting hyperactivity of individual neurons in the auditory cortex. Here, to investigate whether more neurons were activated in the auditory cortex of *Fmr1* KO mice, we quantified the density of c-Fos+ cells (Fig. 3). A 400 μm wide rectangular window that spanned the length of cortical layers I-VI was used to quantify c-Fos+ cell density (Fig. 3A, B). In the quiet condition (Figure 3C), there were no genotype differences in the number of c-Fos+ cells in the auditory cortex of WT and *Fmr1* KO mice at P21 (U=16, p=0.302) or P34 (U=26, p=0.529; Fig. 3C, left). In the sound exposure condition (Fig. 3D), there was no significant genotype difference in c-Fos+ cell density at P21 (U=25, p=0.321). At P34, Mann-Whitney tests showed a significant genotype difference when mice were exposed to 80 dB (U=6, p=0.018), but the number of c-Fos+ cells was lower in the *Fmr1* KO mouse cortex. There was no difference for the 90 dB sound level (U=33, p=0.364).

Electrophysiology

Extracellular single unit recordings were obtained from the IC in both genotypes at three different developmental ages: P14, P21, and P30. Spontaneous activity, rate-level functions, frequency tuning curves, and responses to amplitude-modulated tones were compared across age and genotype.

Spontaneous activity of IC neurons shows CF-specific genotype differences

Spontaneous activity was measured by counting the number of spikes over 20 repetitions of the recording window (250 ms) with no sound stimulus. The average spontaneous activity across all recorded neurons for each genotype and age was then used in a two-way ANOVA (age and genotype as factors) to identify statistical differences. The overall spontaneous activity in the IC was low, likely due to the anesthesia (Fig. 4A). However, it was possible to detect a significant main effect of age ($F(2,499)=11.153$, $p=0.000018$) with Bonferroni post-hoc comparison showing a reduction in spontaneous activity with age (P14 vs P21, $p=0.024$; P14 vs P34, $p=0.000007$; and P21 vs P34, $p=0.124$). There was no main effect of genotype ($F(1, 499)=2.333$, $p=0.127$) or significant genotype x age interaction ($F(2,499)=1.186$, $p=0.306$). Thus, when all the neurons were considered together, spontaneous activity decreased during development in the IC, with no genotype differences.

Because there were regional genotype differences in the c-Fos+ cell density in the IC, we analyzed the electrophysiology data by classifying neurons according to CF, with low and high CF groups separated with a 20 kHz cut-off range. We chose the 20 kHz cut-off frequency because the IC tonotopic map splits approximately into two halves at this CF (Felix II et al., 2007). The full statistics for the CF-classified data are provided in

Table 2. *Fmr1* KO neurons with CF<20 kHz produced more spontaneous spikes than their WT counterparts. There was an interaction between age and genotype, but no main effect of age. For neurons with CF≥20 kHz, we observed no main effect of genotype or significant genotype x age interaction. A significant main effect of age was present, with Bonferroni post-hoc comparison showing a decrease in spontaneous activity with age (P14 vs P21, p=0.000182; P14 vs P34, p<0.0001; P21 vs P34, p=0.015) (Fig. 4B). In terms of spontaneous activity in the IC, these data indicate a larger effect of genotype in neurons with CF<20 kHz, and an effect of age in neurons with CF≥20 kHz.

Minimum thresholds of IC neurons show CF-specific genotype differences

We next compared minimum threshold (MT), defined as the lowest sound level that evoked a response to tones. When all neurons were considered regardless of CF, there was no significant main effect of genotype (F(1,501)=1.834, p=0.176) (Fig. 4C). Analysis demonstrated a significant genotype x age interaction (F(2,501)=3.818, p=0.023) and a main effect of age (F(2,501)=11.586, p=0.000012) with Bonferroni post-hoc (P14 vs P21, p=0.000115; P14 vs P34, p=1.00; P21 vs P34, p=0.000037), showing the lowest average MT at P21 compared to P14 and P34.

When separated by CF (Table 2), neurons with CF<20 kHz showed no main effect of genotype or genotype x age interaction for MT. There was a significant main effect of age with Bonferroni post-hoc analysis showing a difference in MT between P14 vs. P21 (p=0.001) and P21 vs. P34 (p<0.0001), but not for P14 vs. P34 (p=0.261) (Fig. 4D). For neurons with CF≥20 kHz, a significant main effect of genotype was seen with a lower MT in *Fmr1* KO compared to WT IC. There was no genotype x age interaction. A

main effect of age (p<0.0001) was also observed for MT with Bonferroni post-hoc comparison showing a difference between P14 vs P21 (p=0.000005) and P14 vs P34 (p=0.007), but not P21 vs P34 (p=0.105) (Fig. 4D). These data suggest that reduced MT in high CF neurons may underlie auditory hyper-responsiveness in *Fmr1* KO mice.

IC neurons in *Fmr1* KO mice are hyper-responsive to tones

Response magnitude to 20 repetitions of the CF tone was measured and compared across age and genotype. For all neurons combined (Fig. 5A), the average response magnitude at MT + 15 dB (15 dB above threshold) showed no significant genotype x age interaction (F(2,481)=1.495, p=0.225). There was a significant main effect of genotype with more spikes/stimulus in *Fmr1* KO mice compared to WT mice (F(1,481)=5.249, p=0.022). There was also a main effect of age (F(2,481)=6.257, p=0.002) with Bonferroni post-hoc comparisons being significant for P21 vs P34 (p=0.004) and P14 vs P34 (p=0.005), but not for P14 vs P21 (p=1.00) (Fig. 5A). Sound-evoked responses were reduced with age in both WT and KO IC. For CF tone responses at MT + 30 dB (Fig. 5B), there was a significant genotype x age interaction (F(2,477)=4.303, p=0.014) and a significant main effect of genotype (F(1,477)=4.772, p=0.029), with *Fmr1* KO mouse neurons responding with more spikes than WT neurons. There was a significant main effect of age (F(2,477)=6.313, p=0.002) with Bonferroni post-hoc tests revealing no significant differences in P14 vs P21 (p=1.00), but a significant reduction with age in P21 vs P34 (p=0.001) and P14 vs P34 (p=0.019) comparisons.

For neurons with CF<20 kHz (Table 2), responses to tones at MT + 15 dB showed a significant main effect of genotype with *Fmr1* KO neurons responding more

than WT neurons (Fig. 5C). There was no significant main effect of age or genotype x age interactions. Similarly, for tones presented at MT + 30 dB (Fig. 5D), there was a significant main effect of genotype (Fig. 5D), but no main effect of age or genotype x age interactions.

For neurons with CF≥20 kHz, response magnitude for tones presented at MT + 15 dB, (Fig. 5C) showed a main effect of age. There were no significant differences in Bonferroni post-hoc comparison of P14 vs P21 (p=1.00), but a significant difference was present for the P14 vs P34 (p=0.022) and P21 vs P34 (p=0.003) comparisons. There was no main effect of genotype or genotype x age interactions. At MT + 30 dB (Fig. 5D), there was no main effect of genotype. There was a main effect of age with no significant difference using Bonferroni post-hoc comparisons in P14 vs P21 (p=1.000) and P14 vs P34 (p=0.092), but a significant difference in P21 vs P34 comparisons (p=0.003). A significant genotype x age interaction was also present.

Overall, the number of action potentials elicited by the CF tone was higher in IC of *Fmr1* KO mice for neurons with CF<20 kHz. IC neurons with CF≥20 kHz showed a reduction in response magnitude with age, but no genotype differences. These results were similar to those seen with spontaneous activity.

Rate-level functions of IC neurons are not different between genotypes

Higher response magnitude at lower sound levels may predispose the *Fmr1* KO mice to AGS at high sound levels (Faingold and Boersma Anderson, 1991). To quantify the relationship between increasing sound levels and response magnitude, rate-level functions were plotted for CF tone responses measured with sound levels between 10 and

494 90 dB SPL (e.g., Fig. 6A). Percent turnover (%TO) is a measure of the non-monotonicity
495 of rate-level functions and indicates the extent to which responses are reduced after
496 reaching a peak with increasing sound levels. We hypothesized that %TO is lower in
497 *Fmr1* KO mice compared to WT mice. The dynamic range (DR) is the range of sound
498 levels over which the response increases from 10% to 90% of maximum. We tested the
499 hypothesis that DR was narrower in the *Fmr1* KO mouse IC than in WT mice. This
500 would cause the *Fmr1* KO mouse IC to be activated to near maximal levels even with
501 small increases in sound level.
502 When all neurons were combined across CF (Fig. 6B), there was no main effect of
503 genotype in the %TO ($F(1,482)=0.559$, $p=0.455$) or genotype x age interactions
504 ($F(2,482)=0.716$, $p=0.489$). There was a significant effect of age ($F(2,482)=6.422$,
505 $p=0.002$) with Bonferroni post-hoc significant differences at P14 vs P21 ($p=0.011$) and
506 P14 vs P34 ($p=0.004$), but not at P21 vs P34 ($p=1.00$). Percent TO decreased with age,
507 indicating that neurons become more monotonic with age. For DR as well (Fig. 6C),
508 there was no main effect of genotype ($F(1,356)=0.601$, $p=0.439$) or genotype x age
509 interactions ($F(2,356)=1.935$, $p=0.146$). There was a main effect of age ($F(2,356)=3.522$,
510 $p=0.031$). Bonferroni post-hoc comparisons did not show any specific pairwise
511 differences (P14 vs P21, $p= 0.189$; P14 vs P34, $p=0.129$; and P21 vs P34, $p=1.00$).
512 When the data were split by CF (Table 3), the statistical trends were similar to
513 those observed for the full dataset. For %TO, neurons with CF<20 kHz showed no main
514 effects of genotype or genotype x age interaction. There was a main effect of age with
515 Bonferroni post-hoc comparisons showing no significant pairwise differences (P14 vs
516 P21, $p=0.061$; P14 vs P34, $p=0.138$; and P21 vs P34, $p=1.00$). For neurons with CF≥20

kHz, there was a decrease in %TO in *Fmr1* KO mice compared to WT mice. This indicates neurons were more monotonic in WT mice, in a disagreement with our original hypothesis. There was no significant genotype x age interaction or main effect of age. For the dynamic range measurement, neurons with CF<20 kHz showed no main effect of genotype or genotype x age interaction. There was a significant main effect of age with Bonferroni post-hoc comparisons showing differences between P14 and P21 (p=0.004) and P14 and P34 (p=0.013), but not between P21 and P34 (p=1.00). For neurons with CF≥20 kHz, there were no main effects or interactions. Taken together, these data suggest that rate-level relationships in IC neurons were relatively normal in the *Fmr1* KO mice and may not contribute to auditory hypersensitivity in FXS.

Low frequency IC neurons show longer response latency in *Fmr1* KO mice

The median first spike latency of IC neuron responses to CF tone was measured at MT + 15 dB and MT + 30 dB (Fig. 7). For MT + 15 dB data, a two-way ANOVA showed a significant main effect of age for latency ($F(2, 477)=35.43$, $p<0.0001$, Fig. 7A). There was no significant main effect of genotype ($F(1,477)=0.613$, $p=0.434$) or genotype x age interactions ($F(2,477)=1.262$, $p=0.284$). Bonferroni post-hoc analysis revealed a significant difference in the P14 vs P21 ($p<0.0001$), P14 vs P34 ($p<0.0001$), and P21 vs P34 ($p=0.00082$) comparisons, with latencies decreasing with age. Likewise, for CF tones presented at MT + 30 dB (Fig. 7B), there was a significant main effect of age ($F(2,475)=114.773$, $p<0.0001$) with Bonferroni post-hoc comparison at P14 vs P21 ($p<0.0001$), P14 vs P34 ($p<0.0001$), and P21 vs P34 ($p<0.0001$) pairs, showing

539 decreasing latency with age. There was no main effect of genotype ($F(1,475)=0.904$,
540 $p=0.342$) or genotype x age interactions ($F(2, 475)=0.087$, $p=0.917$).
541 When neurons were classified by CF (Table 3), neurons with CF<20 kHz showed
542 a significant main effect of genotype with longer latency in the KO compared to WT for
543 tones with sound level of MT + 15 dB (Fig. 7C). There was also a main effect of age with
544 Bonferroni post-hoc comparison of P14 vs P21 ($p=0.0042$), P14 vs P34 ($p=0.00018$), and
545 P21 vs P34 ($p=1.00$) pairs, showing decreasing latency with age. There was no
546 significant difference in genotype x age interaction. For neurons with CF≥20 kHz, there
547 was no significant main effect of genotype or genotype x age interactions. There was a
548 significant main effect of age with Bonferroni post-hoc analysis showing differences for
549 P14 vs P21 ($p<0.0001$), P14 vs P34 ($p<0.0001$) and P21 vs P34 ($p=0.0053$) pairs, with
550 latency decreasing with age.
551 Similarly, at MT + 30 dB (Fig. 7D), neurons with CF<20 kHz showed a main
552 effect of genotype and a main effect of age ($p<0.0001$) with Bonferroni post-hoc
553 comparisons showing differences for the P14 vs P21 ($p=0.0023$), P14 vs P34 ($p<0.0001$)
554 and P21 vs P34 ($p=0.000055$) pairs, with latency decreasing with age. There was no
555 significant genotype x age interaction. For neurons with CF≥20 kHz, there was a
556 significant main effect of age with Bonferroni post-hoc comparisons showing differences
557 for the P14 vs P21 ($p<0.0001$), P14 vs P34 ($p<0.0001$) and P21 vs P34 ($p<0.0001$) pairs,
558 with latencies decreasing with age. There was no significant main effect of genotype or
559 genotype x age interactions. Thus, the median first spike latency in response to CF tones
560 decreased during development across all CFs, with genotype differences (slower latency
561 in *Fmr1* KO neurons) seen for neurons with CF<20 kHz.

562

563 **Low frequency IC neurons in the *Fmr1* KO mice show broader frequency tuning**

564 To determine if frequency selectivity is affected in the IC of *Fmr1* KO mice, we
565 performed a genotype and age comparison of frequency response area bandwidths (BW)
566 at three different sound levels: 10, 20, and 30 dB above MT (BW10, BW20, and BW30,
567 respectively). Frequency response areas (e.g., Fig. 8A) were plotted by measuring the
568 number of action potentials to 20 repetitions of each frequency/sound level combination
569 ranging from 4-48 kHz (4 kHz steps) and 10-90 dB SPL (10 dB steps). The bandwidth of
570 the frequency response area at 10 (BW10), 20 (BW20) and 30 (BW30) dB above the
571 neuron's MT was measured to quantify frequency selectivity.

572 For BW10, there was a significant genotype x age interaction ($F(2,307)=4.971$,
573 $p=0.008$) (Fig. 8B), but no main effect of genotype ($F(1,307)=0.679$, $p=0.410$) or age
574 ($F(2,307)=2.556$, $p=0.079$). A main effect of genotype was seen for BW20 (Fig. 8B),
575 with broader tuning curves in *Fmr1* KO mice compared to WT mice ($F(1,307)=3.927$,
576 $p=0.048$). There was also a significant main effect of age ($F(2,307)=6.096$, $p=0.003$) with
577 Bonferroni post-hoc test showing a significant difference in P14 vs P21 ($p=0.002$) and
578 P14 vs P34 ($p=0.024$), but not P21 vs P34 ($p=1.00$). There was no significant genotype x
579 age interaction ($F(2,307)=1.095$, $p=0.336$). For BW30 (Fig. 8B), there was a significant
580 effect of age ($F(2,307)=12.276$, $p=0.000007$) with Bonferroni post-hoc showing a
581 difference in P14 vs P21 ($p=0.000018$) and P14 vs P34 ($p=0.000066$), but not in the P21
582 vs P34 ($p=1.00$) groups. There was no main effect of genotype ($F(1,307)=0.860$,
583 $p=0.354$) or genotype x age interaction ($F(2,307)=0.032$, $p=0.968$). Thus, when all
584 neurons were considered together, genotype difference was seen only for BW20 with

585 *Fmr1* KO neurons showing broader tuning. For BW20 and BW30, we observed a
586 narrowing of tuning curves with developmental age.

587 When separated by CF, neurons with CF<20 kHz (Fig. 8C, Table 4) were more
588 broadly tuned in the *Fmr1* KO IC compared to WT IC at BW10, BW20 and BW30. For
589 BW10, BW20 and BW30, there was no significant genotype x age interaction or main
590 effect of age. Neurons with CF≥20 kHz (Fig. 8D) showed no main genotype or age
591 effects for BW10, BW20 or BW30. A genotype x age interaction was only seen for
592 BW10. Thus, IC neurons with CF<20 kHz, but not higher CF neurons, showed a broader
593 tuning in *Fmr1* KO compared to WT mice, which was more pronounced at P21. Yet
594 again, these data indicate that IC neurons with CF<20 kHz show more genotype
595 differences than neurons with CF≥20 kHz.
596
597 **IC neurons showed stronger responses to amplitude modulated tones in *Fmr1* KO**
598 **than WT mice**
599 The rate modulation transfer function (rMTF) and temporal modulation transfer
600 function (tMTF) for responses to sinusoidal amplitude modulated (SAM) tones were
601 compared across age and genotype (Fig. 9). The rMTF was analyzed as the average
602 number of spikes per stimulus presentation over the duration of the stimulus. The tMTF
603 was quantified as the degree of synchronization to the modulations measured as vector
604 strengths. Modulation rates of 5, 10, 20, 50, 100, and 200 Hz with carrier frequency
605 centered at CF were used and the SAM tone was presented at MT + 15 dB.
606 For rMTF analysis, a two-way ANOVA (genotype and age as factors) was run for
607 each modulation rate. The main statistics are summarized in Table 5, including analyses

608 of all neurons pooled or separated by CF (20 kHz cut-off). In general, Table 5 and
609 Figures 9 and 10 show a number of significant genotype differences in rMTF driven
610 mostly by increased responses to SAM in the *Fmr1* KO mice. Figure 9 (C-E) also
611 suggests that the increased responses are more prominent at faster modulation rates with
612 *Fmr1* KO IC neurons showing a peak ~50 Hz modulation rates compared to WT neurons,
613 on average. Neurons with CF<20 kHz also show more consistent genotype differences
614 across modulation rates (Table 5, Fig. 10). No consistent patterns were seen for main
615 effects of age or age x genotype interactions. Together, we interpret these data to indicate
616 that responses to modulated tones are increased in the *Fmr1* KO mice.
617 For tMTF (Table 6, Fig. 9F-H, 11), main effects of genotype were rare (seen only
618 for 10 Hz modulation rate), and the other effects do not show a consistent pattern of
619 specific developmental change or genotype x age interactions. This suggests that
620 temporal response properties of IC neurons when tested with SAM tones are not different
621 in *Fmr1* KO mice compared to WT, and are unlikely to contribute to abnormal auditory
622 sensitivity.
623
624 **Tonotopy**
625 We quantified the development and possible genotype differences in tonotopy in
626 the IC and observed the expected dorsal to ventral increase in CF representation (Felix
627 and Portfors, 2007) at all three developmental ages (Fig. 12) and across genotypes. The
628 CF representation was mostly <30 kHz at P14 and expanded to include more neurons
629 with CF>30 kHz at P21 and P34. There was no significant difference in the distribution
630 of CFs across genotypes at any age (P14: $t(159)=0.831$, $p=0.406$), (P21: $t(164)=0.788$,

631 p=0.431), and (P34: t(188)=0.589, p=0.555). Together, these data suggest that CF-
632 specific susceptibilities in *Fmr1* KO mice are not due to abnormal development of
633 tonotopy.
634
635 **DISCUSSION**
636 Based on c-Fos+ cell density analysis, our results indicate that more IC neurons
637 were activated in the *Fmr1* KO mice compared to WT following sound exposure at both
638 P21 and P34. Genotype differences in the density of c-Fos+ cells are also observed in the
639 PP and SGN divisions of the MGB. *In vivo* single unit recordings show that IC neurons
640 of *Fmr1* KO mice are more responsive to both tone bursts and amplitude-modulated
641 tones, and show broader frequency tuning curves than their WT counterparts. In general,
642 genotype differences emerge between P14 and P21, with a stronger effect on neurons
643 with CF<20 kHz, compared to neurons with higher CF. Together, these data suggest that
644 the IC is a major contributor to early developmental auditory hyper-responsiveness in
645 FXS.
646
647 *Increased density of c-Fos+ cells in the IC of Fmr1 KO mice at both P21 and P34*
648 The genotype difference in c-Fos+ cell density was apparent in the dorsolateral
649 half of the IC at P21, and shifted to the ventromedial half of the IC (adjacent to the
650 periaqueductal gray) at P34. Chen and Toth (2001) previously examined c-Fos
651 expression in response to sounds in *Fmr1* KO mice using sound levels that caused AGS
652 in some of the mice. When AGS was induced in *Fmr1* KO mice, there was an increase in
653 c-Fos expression in KO compared to WT mice in the dorsal nucleus of the lateral

654 lemniscus, posterior intralaminar nucleus, periaqueductal grey, and MGm. However,
655 because the *Fmr1* KO mice showed seizures and the WT mice did not, motor responses
656 associated with increased AGS-related movement likely contributed to the genotype
657 differences in c-Fos+ cell density (Yang et al., 2020). To overcome this confound, the
658 sound stimulus in our study was in the 80-90 dB range, which did not induce AGS in any
659 of the mice used for c-Fos analysis. Under these conditions, we found a genotype
660 difference in the density of c-Fos+ cells in the IC suggesting that the extent of activity in
661 the IC may be a correlate of sensory hypersensitivity in early development.
662 Dorsomedial IC represents low CFs while ventromedial IC represents higher CFs.
663 Hyper-responsiveness is seen in *Fmr1* KO IC in response to both tone bursts and AM
664 tones for neurons with CF<20 kHz at both P21 and P34. Neurons with CF≥20 kHz do
665 not show considerable differences in response magnitude at either P21or P34. This lack
666 of spatiotemporal correlation between the c-Fos data and single unit data suggests that the
667 increased density of c-Fos+ cells and increased response magnitudes may contribute
668 independently to hypersensitivity.
669 Analysis of the density of c-Fos+ cells in the MGB suggests a point of interaction
670 between abnormal sensory processing and anxiety in FXS during early development (Cho
671 et al., 2012). The MGm is a region projecting to all cortical layers and to the amygdala.
672 The SGN is a region that receives multisensory inputs and also projects to the amygdala
673 (LeDoux et al., 1991). The peripeduncular (PP) nucleus integrates auditory, motor and
674 hypothalamic signals (Arnault and Roger, 1987). The recruitment of more cells may
675 underlie a stronger activation of auditory-limbic-motor pathways which may lead to

676 behavioral anxiety phenotypes in response to daily environmental sounds in FXS (Miller
677 et al., 1999; Reinhard et al., 2019).
678 We did not observe an increase in sound-evoked c-Fos+ cell density in the
679 auditory cortex at P21 or P34. While the IC showed both higher density of activated c-
680 Fos+ cells and increased response magnitude in the *Fmr1* KO mice at this age, the
681 auditory cortex only shows the increased response magnitude (Wen et al., 2018). When
682 *Fmr1* KO mice are most sensitive to AGS (~P21), our data suggests that the IC plays a
683 stronger role than the cortex. This is consistent with the role of IC in AGS generation in
684 rats genetically prone to epilepsy (Faingold 2002) and in the *Fmr1* KO mice (Gonzalez et
685 al., 2019).
686
687 *Single unit recordings reveal hypersensitivity to sounds in the IC of Fmr1 KO mice*
688 *In vivo* electrophysiological recordings in the IC at P14, P21, and P34 showed that
689 the *Fmr1* KO neurons produce increased responses to tone bursts and amplitude-
690 modulated tones and had broader frequency tuning curves compared to age-matched WT
691 neurons. Low frequency tuned neurons (CF<20 kHz) show greater genotype differences
692 compared to neurons with CF≥20 kHz. Rotschafer and Razak (2013) suggested that a
693 possible mechanism of increased synchrony and hypersensitivity to sounds may be linked
694 to broader frequency tuning curves of individual neurons in *Fmr1* KO mice. This is
695 because more neurons would be activated in response to a single tone frequency if tuning
696 curves were broader, and overlapped more. IC neurons show broader tuning curves in
697 *Fmr1* KO mice than in WT, suggesting that more IC neurons will respond synchronously
698 to sounds. These data suggest that the IC is a major source of auditory hyper-

699 responsiveness in FXS during development through increased response magnitudes and a
700 greater number of synchronously activated neurons.
701 Faingold and Anderson (1991) suggested that abnormal inhibition with increasing
702 sound level in IC neuronal response may lead to AGS in rats genetically susceptible to
703 epilepsy. Therefore, we quantified rate-level responses across age and genotype. In the
704 *Fmr1* KO mice, there were no genotype differences in either the non-monotonicity of
705 responses or the dynamic range. These data do not support the hypothesis that AGS
706 susceptibility of *Fmr1* KO mice is due to abnormal rate-level relationships in the IC.
707 Given the CF-specific genotype effects observed and because of a previous study that
708 showed tonotopic gradients of ion channel expression may be affected in the lower
709 auditory brainstem, we hypothesized that development of tonotopy may show genotype
710 differences (Ruby et al., 2015; Strumbos et al., 2010). However, there were no genotype
711 differences in tonotopy indicating that map formation, and the underlying guidance cues
712 (Cramer and Gabriele, 2014) are relatively normal in the IC of *Fmr1* KO mice.
713 Therefore, increased response to un-modulated and amplitude-modulated tones, broader
714 frequency tuning curves, and increased recruitment of active cells seem to be the major
715 IC phenotypes associated with auditory hyper-responsiveness at P21.
716
717 *Development of IC responses in WT and Fmr1 KO mice*
718 Although the major focus of our study was on the *Fmr1* KO mice, the WT data
719 are useful to compare with previous studies of IC development. Our data are consistent
720 with previous findings of shortening latencies, decreasing thresholds, sharpening
721 frequency tuning and increasing high frequency representation in the developing IC

(Aitkin and Moore, 1975; Schnerson and Willott, 1979; Romand and Ehret, 1990; Ehret and Romand, 1992). In addition, we show that both spontaneous and tone-driven response magnitudes of IC neurons decline with age. This was also true for responses to amplitude modulated tones. When IC neurons with CF<20 kHz are considered, there was no main effect of age on the rMTF to AM tones (Table 5). However, IC neurons with CF≥20 kHz show reduced spike counts with age at multiple modulation rates. This suggests that AM responses mature more slowly in the high frequency IC neurons. Taken together, these data are in alignment with both the development of the cochlea, and the maturation of inhibitory circuitry that shape frequency tuning and response magnitudes of IC neurons (Fuzessery and Hall, 1996; Le Beau et al., 1996; Zhang and Kelly 2003; Hurley et al., 2008).

A number of age x genotype interactions were observed in this study suggesting that some of the differences may be present only at certain ages. A notably important pattern in the data was that the IC properties are comparable between *Fmr1* KO and WT mice at P14, but begin to diverge at P21. Sound driven responses begin to occur ~P10-11 in the IC. In the first 2 weeks of life, refinement of both extrinsic ascending and intrinsic local connectivity patterns depend mostly on spontaneous activity driven by the cochlea (Gabriele et al., 2000a). Patterns of extrinsic inputs to the IC appear mature at or before hearing onset (Gabriele et al., 2000b, Henkel et al., 2007; Fathke and Gabriele, 2009). Our data suggest that this developmental process is relatively normal in *Fmr1* KO mice. Between P14 and P21, sound-driven refinements of excitatory local inputs dominate such that inhibition becomes relatively stronger (E:I ratio declines from P14-21 in WT mice, Sturm et al., 2014). This will sharpen frequency tuning and reduce response magnitudes

745 during development. This process seems to be affected in *Fmr1* KO mice. Abnormal
746 sound-driven refinement may result in elevated response magnitude, broader frequency
747 tuning and consequently hypersensitivity. Grimsley et al., (2013) suggested that the local
748 circuit connectivity may shape responses of IC neurons to increasing sound levels.
749 Therefore, abnormal local IC circuit refinement may also be implicated in AGS.
750 Whether this is due to abnormal refinement of excitatory connections and/or abnormal
751 development of inhibition remains to be investigated.
752 Another main observation is that neurons with CF<20 kHz appear to be more
753 hypersensitive than neurons with CF≥20 kHz. The underlying mechanisms for this
754 frequency dependence are unclear, but suggest abnormal GABA responses in the IC of
755 *Fmr1* KO mice. Based on the IC tonotopic gradient, neurons with increasing CF are
756 found more ventrally in the IC and most neurons with CF<20 kHz are likely to be within
757 1,000 μm from the dorsal surface (~50% of total dorso-ventral depth (Felix and Portfors,
758 2007). IC neurons receive both GABA and glycine inhibitory inputs. Glycine may be
759 more dominant in shaping inhibition in ventral, high-CF regions of the IC (Choy
760 Buentello et al., 2015; Merchán et al., 2005; Sanes et al., 1987). GAD67-labeled inputs
761 appear to dominate more in the dorso-medial regions of the IC (Choy Buentello et al.,
762 2015), suggesting a more prominent role for GABA in the dorsal half of the IC. This may
763 suggest a deficit in GABAergic inhibition, because most deficits were observed in low
764 CF neurons in the dorsolateral region of the IC. GABAa receptor deficits in the IC are
765 related to AGS in rats that are genetically susceptible to epilepsy (Faingold, 2002). In
766 addition, down-regulated tonic GABAa currents and a decrease in GABAa receptors
767 were reported in *Fmr1* KO mice (Curia et al., 2009; D'Hulst et al., 2006), suggesting

768 impaired GABA-mediated inhibition in FXS. GABAergic inputs shape firing rates of IC
769 neurons (Palombi and Caspary, 1996). Whether glycinergic inhibition is affected in the
770 IC is unclear, but Garcia-Pino et al. (2017) showed no impact on such inhibition in the
771 lower brainstem of *Fmr1* KO mice. Together, these studies suggest the CF-dependent
772 susceptibility of IC to hyper-responsiveness in early development may be related to
773 GABA dysfunction in *Fmr1* KO mice.
774
775 **System-wide deficits in auditory processing in FXS**
776 Given the consistent and debilitating auditory hypersensitivity in individuals with
777 FXS, there is an increasing interest in understanding the underlying the circuit and
778 cellular pathophysiology across the auditory system and across development (McCullagh
779 et al., *In Press*). FMRP is expressed at multiple levels of the auditory system from the
780 cochlear nucleus to the auditory cortex. Global deletion of *Fmr1* would affect the
781 development and function of each of these auditory processing stages. Neurons in the
782 lateral superior olive (LSO) of the brainstem show enhanced excitatory synaptic input
783 strength through increased convergence of cochlear nucleus input early in development
784 (Garcia-Pino et al., 2017). LSO neurons showed increased firing rates and broader
785 frequency tuning curves. The abnormal IC responses may, therefore, originate in the
786 lower brainstem. However, this needs to be verified by comparing lower brainstem and
787 IC recordings conducted at similar ages. In the medial nucleus of the trapezoid body
788 (MNTB), one of the major sources of inhibition to the LSO, the tonotopic gradient of
789 Kv3.1b potassium ion channel is significantly flatter in *Fmr1* KO, compared to WT mice
790 (Strumbos et al., 2010). Modeling (Strumbos et al., 2010) and electrophysiological

791 (Brown et al., 2010) data suggest an impact on temporal precision in MNTB of *Fmr1* KO
792 mice. This may be limited to the MNTB, as our IC data do not reveal any genotype
793 differences in tMTF in response to amplitude modulated tones, suggesting that single
794 neuron phase locking is not affected in the IC. Cell sizes were also reduced and VGAT
795 expression is elevated in the MNTB of the *Fmr1* KO mice suggesting increased
796 inhibitory input and disinhibition of the LSO (Rotschafer et al., 2015).
797 The auditory cortex has received considerable attention in FXS. Rotschafer and
798 Razak (2013) showed increased response magnitude and broader frequency tuning in the
799 auditory cortex of *Fmr1* KO mice. Wen et al., (2018) showed that such responses are
800 seen at P21, but not at P14, suggesting the origin of hyper-responsivity in this
801 developmental time frame when cortical properties mature (Oswald and Reyes, 2008,
802 2011). The IC also shows greater genotype difference in response magnitudes at P21, but
803 not P14, suggesting that the cortical hyper-responsivity may be inherited from subcortical
804 sites, including the IC. Similar developmental studies have not been performed in the
805 medial geniculate body.
806 Consistent with abnormal inhibition, Wen et al. (2018) showed that increased
807 matrix metalloproteinase-9 (MMP-9) in the auditory cortex may lead to abnormal
808 development of perineuronal nets (PNN) and parvalbumin (PV) positive inhibitory
809 interneurons. Loss of PNNs will reduce excitability of PV cells resulting in reduced
810 network inhibition. This suggests that at least part of the cortical deficit arises due to
811 PV/PNN deficits that are local to cortex, and not inherited from the IC. This notion was
812 further supported by a recent study that showed that removal of *Fmr1* only from forebrain
813 excitatory neurons using the *Nex1* promoter results in enhanced low gamma oscillations

814 in the cortex indicating local cortical circuit deficits (Lovelace et al., 2019). Interestingly,
815 however, enhanced high gamma seen in previous cortical recordings from global *Fmr1*
816 KO mice was not present when *Fmr1* was removed only from forebrain neurons. This
817 suggests a combination of cortical and subcortical contributions give rise to the various
818 auditory processing phenotypes studied in the *Fmr1* KO mice. The present study
819 identifies the IC as a potentially strong hub of hypersensitive responses, at least in early
820 development.
821
822 Methodological issues
823 For the c-Fos analysis, up to 4 mice were exposed together in a cage. Importantly,
824 they were always of the same genotype and age range when tested together. The control
825 (WT) group and the *Fmr1* KO group were tested with identical methods. Therefore, any
826 group testing effects must affect each genotype similarly. However, any differences in
827 social vocalizations or movement related sounds (walking, running, etc) across genotypes
828 may potentially affect c-Fos expression in auditory nuclei. Future studies will test one
829 mouse at a time, and quantify movement related sounds to address these caveats.
830 No counterstaining was used to distinguish layers of the cortex, divisions of the
831 MGB or the nuclei of the IC. The distinct areas within each auditory region were
832 identified based on mouse brain atlas. Future studies with cytoarchitecture counterstains
833 are needed to identify specific sub-nuclei with more precision. Electrophysiological
834 responses were recorded under anesthesia, and this may have reduced the spiking activity
835 of individual neurons. Whether the reported hyperactivity of IC neurons in *Fmr1* KO

836 mice may actually be an under-estimate remains to be identified with recordings
837 conducted in awake mice.
838 We did not perform analysis of age-related changes in the density of c-Fos+ cells
839 to identify any differences in developmental trajectories across the genotypes. The
840 reason for this is the use of different sound levels at the two ages studied. We used the
841 loudest sound levels that did not cause AGS at each age tested. The 85 and 90 dB levels
842 used were ~5 dB below AGS threshold at P21 and P34, respectively. But they were not
843 matched in absolute sound levels.
844
845 Conclusions
846 We found region-specific deficits in both the density of c-Fos+ cells and response
847 properties in the IC of developing *Fmr1* KO mouse. Most of the deficits were seen at
848 P21, the time of high AGS susceptibility. In addition, the main differences were in
849 dorsolateral IC and in neurons tuned to lower frequencies in the IC. This implies that
850 FMRP affects differently low and high frequency regions of IC. Future studies should
851 examine AGS with stimuli that are low-pass or high-pass filtered at ~20 kHz to determine
852 if the *Fmr1* KO mice are more sensitive to low-frequency sounds during development.
853 The lack of electrophysiological deficits at P14 indicates abnormal experience dependent
854 plasticity between P14-P21, similar to that seen in the auditory cortex (Wen et al., 2018).
855 In addition, studies on the cognitive and social impacts of early life IC dysfunction are
856 needed to address development of autism related behaviors in *Fmr1* KO mice.
857 It is important to consider that in neurodevelopmental disorders, it is difficult to
858 disambiguate direct effects of genetic changes, the effects of altered experiences of the

859 animal caused by the genetic change, and the compensatory plasticity mechanisms
860 generated in the brain (Antoine et al., 2019; Bulow et al., 2019). In fact, many
861 phenotypes observed in FXS (human and mice) are only seen transiently or fluctuate
862 during development (Meredith et al., 2012; Vislay et al., 2013; Wen et al., 2019). Even
863 transient disruptions during early development can have long lasting impact. In the case
864 of auditory hypersensitivity in *Fmr1* KO mice, divergence towards hyper-responsiveness
865 appears to occur between P14 and P21. Our data point to the importance of studies to
866 track the developmental trajectories of phenotypes (Razak et al., *In Press*). This will aid
867 in identifying optimal treatment windows during development for clinical trials in FXS.
868
869 **Figure Legends**
870 **Figure 1: c-Fos+ cell density is increased in the inferior colliculus (IC) of *Fmr1* KO**
871 **mice.** (A, B) Example photomicrographs of c-Fos immunoreactivity in the IC obtained
872 from P21 WT (A) and P21 *Fmr1* KO mice (B) following sound exposure (85 dB). (C, D)
873 Example photomicrographs of c-Fos immunoreactivity in the IC at P34 following 90 dB
874 sound exposure of WT (C) and *Fmr1* KO mice (D). Rectangular boxes in panels A-D
875 show counting windows (400 μm width) that span the IC in a dorsolateral to
876 medioventral direction. (E) For the 0-50% counting window (dorsolateral half), there
877 were no significant genotype differences in the density of c-Fos+ cells at both ages in the
878 quiet group. (F) In the sound-exposed group, for the 0-50% window, there was a
879 significant increase in c-Fos+ cell density at P21 in *Fmr1* KO mice (*, p=0.010) and a
880 genotype effect at P34 (p=0.028). (G) In the 51-100% window (medioventral half), there
881 was a significant decrease in c-Fos+ cell density in the *Fmr1* KO mice at P34 under the

quiet condition (* p=0.004). (H) For the sound-exposed group, there was no genotype difference at P21 in 51-100% window of the IC. At P34, there was significant increase in c-Fos+ cell density in *Fmr1* KO compared to WT (p=0.030) mice. Error bars show s.e.m.

Figure 2: Sub-division specific genotype differences in c-Fos+ cell density in the medial geniculate body (MGB). (A) Example photomicrographs of c-Fos immunoreactivity in the MGB of WT and *Fmr1* KO mice obtained at P21. (B) Box and Whisker plot of c-Fos+ cell density in the quiet groups at P21 and P34. (C) Box and Whisker plot of c-Fos+ cell density in the sound-exposed groups at P21 and P34. Scale bar=200 μm.

Figure 3: Genotype comparisons of c-Fos+ cell density in the auditory cortex. (A-B) Example photomicrographs of sound driven c-Fos immunoreactivity in auditory cortex of P21 WT (A) and *Fmr1* KO (B) mice. All 6 cortical layers are shown in these panels with a pial surface at the top of the image. Scale bar=100 μm. (C) Box and Whisker plot of c-Fos+ cell density in the quiet condition. (D) Box and Whisker plot of c-Fos+ cell density in the sound-exposed condition.

Figure 4: Spontaneous activity and minimum threshold of *Fmr1* KO and WT IC neurons at P14, P21 and P34. The graphs in (A) and (B) show the average number of spikes per acquisition window (250 msec, 20 repetitions) in the absence of any stimulus. (A) A two-way ANOVA (age x genotype) shows a main effect of age (p=0.000018), with spontaneous firing rate decreasing across development. (B) For neurons with CF < 20

kHz, a two-way ANOVA revealed significant interaction between genotype x age (p=0.008) and significant main effects of genotype, but no significant main effect of age (Genotype: p=0.04, Age: p=0.08). For neurons with CF≥20 kHz, there was no significant genotype x age interaction or main effects of genotype (p=0.949, p=0.335, respectively). There was a significant main effect of age (p=0.000004). (C) The average minimum threshold at CF for neurons in IC showed no main effects of genotype (p=0.176). There was a significant interaction between genotype x age and a main effect of age (p=0.023, p=0.000012, respectively). (D) For neurons with CF<20 kHz, there was no significant genotype x age interaction or main effect of genotype (p=0.282, p=0.09, respectively). There was a significant main effect of age (p=0.000004). For neurons CF≥20 kHz, there was no significant interaction between genotype x age (p=0.299). There was a significant main effect for both genotype and age (p=0.000005). Error bars show s.e.m.

Figure 5: *Fmr1* KO IC neurons show increased response magnitude to CF tones than WT neurons. (A) Average response magnitude when tested with CF tones at 15 dB above minimum threshold (MT + 15 dB). There was a significant main effect of genotype and age (p=0.022, p=0.002, respectively), but no significant interaction between genotype x age (p=0.225). (B) Average response magnitude when tested with CF tones at 30 dB above minimum threshold (MT + 30 dB). There was a significant interaction between genotype x age (p=0.014), main effect of genotype (p=0.029) and main effect of age (p=0.002). (C) Response magnitude at MT + 15 dB for neurons separated by CF (CF<20 kHz vs. CF≥20 kHz). For neurons with CF<20 kHz, there was no significant genotype x age interaction (p=0.759) or main effect of age (p=0.288). A significant main effect of

928 genotype (p=0.00016) was present. For neurons with CF≥20 kHz, there was a significant
929 main effect of age (p=0.002), but no significant genotype x age interaction (p=0.217) or
930 main effect of genotype (p=0.968). (D) Response magnitude at MT + 30 dB for neurons
931 separated by CF. For neurons with CF<20 kHz, there was no significant interaction
932 between genotype x age (p=0.124) or main effect of age (p=0.2). There was a significant
933 main effect of genotype (p=0.000030). For neurons with CF≥20 kHz, there was a
934 significant interaction between genotype x age (p=0.006) and main effect of age
935 (p=0.005), but there was no significant main effect of genotype (p=0.840). Error bars
936 show s.e.m (*p<0.05).
937
938 **Figure 6: Rate-level responses of IC neurons were mostly unaffected by genotype at**
939 **all ages tested.** (A) An example rate-level response function in a WT IC neuron (P21).
940 Vertical dashed lines from left to right indicate sound level for 10% of maximum
941 response and 90% of maximum response. Dynamic range (DR) was the range of sound
942 levels over which responses increased from 10% to 90% of the maximum response.
943 Percent turnover (%TO) is the degree of non-monotonicity of the rate-level function and
944 measures the extent to which response at the highest sound level tested is reduced
945 compared to the maximum response. In this example, the %TO was ~50%. (B) For %TO,
946 there was no significant genotype x age interaction (p=0.489) or main effect of genotype
947 (p=0.455). There was a main effect of age (p=0.002), with neurons showing reduced
948 %TO (less non-monotonic) with age. (C) Dynamic range of neurons showed a main
949 effect of age (p=0.031), but no significant genotype x age interaction (p=0.146) or main
950 effect of genotype (p=0.439). Error bars show s.e.m.

Figure 7: No genotype differences were observed in median first spike latencies of neuronal response to CF tones. (A) The median first spike latency of responses to CF tone presented at MT + 15 dB showed no significant interaction between genotype x age (p=0.284) or main effect of genotype (p=0.434). There was a significant main effect of age (p<0.0001), with latency decreasing with age. (B) For latencies in response to CF tones at MT + 30 dB, there was no significant genotype x age interaction (p=0.917) or main effect of genotype (p=0.342). There was a significant main effect of age (p<0.0001), with latencies decreasing with age. (C) For neurons with CF<20 kHz, there was no significant interaction between genotype x age (p=0.743) for latencies measured with tones presented at MT + 15 dB. However, there was a significant main effect of genotype (p=0.029) and main effect of age (p<0.0001). For neurons with CF≥20 kHz, there was a significant main effect of age (p<0.001), but no significance in genotype x age interaction or main effect of genotype (p=0.878, p=0.065, respectively). (D) When tested with tones presented at MT+ 30 dB, the median first spike latency for neurons with CF<20 kHz showed significant main effect of genotype and age (p=0.044, p<0.0001, respectively), but no significant genotype x age interactions (p=0.249). For neurons with CF≥20 kHz, there was a significant main effect of age (p<0.0001), but no significant main effect of genotype (p=0.615) or genotype x age interaction (p=0.956). Error bars show s.e.m.

Figure 8: Frequency tuning was broader in the IC of *Fmr1* KO mice compared to WT mice, mainly for neurons with CF<20 kHz. (A) An example frequency response

974 area with tone frequency on the abscissa and sound intensity on the ordinate. The color
975 scale indicates normalized response magnitude for specific frequency-intensity
976 combinations. The bandwidth of frequency selectivity was quantified at 10 (BW10), 20
977 (BW20) and 30 (BW30) dB above the minimum threshold of neurons. (B) When all
978 neurons within each genotype were pooled together, there was no significant main effect
979 of genotype for BW10 ($p=0.410$) or BW20 ($p=0.354$). A significant main effect of
980 genotype was present only for BW20 ($p=0.048$). A significant main effect of age was
981 seen for BW20 ($p=0.003$) and BW30 ($p<0.0001$), but not for BW10 (0.079). (C) For
982 neurons with CF<20 kHz, there was a significant main effect of genotype (BW10
983 ($p=0.039$), BW20 ($p=0.017$), BW30 ($p=0.018$)). There was no genotype x age interaction
984 (BW10 ($p=0.175$), BW20 ($p=0.616$), BW30 ($p=0.68$)) or main effect of age (BW10
985 ($p=0.944$), BW20 ($p=0.515$), BW30 ($p=0.288$)). (D) For neurons with CF≥20 kHz, there
986 was no significant main effect of genotype ($p=0.726$) or age ($p=0.499$). There was a
987 significant genotype x age interaction only for BW10 ($p=0.04$). Error bars show s.e.m.
988

989 **Figure 9: IC neurons show hyper-responsiveness to amplitude modulated tones in**
990 ***Fmr1* KO mice, but phase-locking is normal.** (A) Example of IC neuron response to
991 sinusoidal amplitude modulated CF tone with 20 Hz modulation in a P14 WT mouse. (B)
992 Polar plot example of action potentials for the same neuron along the period of the
993 stimulus. (C1-C3) Rate modulation transfer function (rMTF) in the P14, P21 and P34
994 groups, respectively. (D1-D3) Temporal modulation transfer function (tMTF) in the P14,
995 P21 and P34 groups, respectively. Dashed lines indicate Fmr1 KO mice and solid lines
996 indicate WT mice. Error bars show s.e.m. (* $p<0.05$).

Figure 10: Rate modulation transfer function (rMTF) subdivided into neurons with CF<20 kHz (A1, B1, C1) and CF≥20 kHz (A2, B2, C2). The rows are arranged by postnatal age (P14, P21 and P34). Error bars show s.e.m. *p<0.05).

Figure 11: Temporal modulation transfer function (tMTF) subdivided into neurons with CF<20 kHz (A1, B1, C1) and CF≥20 kHz (A2, B2, C2). The rows are arranged by postnatal age (P14, P21 and P34). Error bars show s.e.m.

Figure 12: No genotype differences were observed in IC tonotopy at any age. Distribution of CF along recording depth in the IC. There were no significant differences between WT and *Fmr1* KO mice at each age group P14 (A), P21 (B), and P34 (C).

Table 1: Window sizes for c-Fos+ cell analysis in the MGB subdivisions.

Medial geniculate body (MGB) subnuclei	Cell count window size (μm)
Suprageniculate Nucleus (SGN)	100 x175
Dorsal division of the MGB (MGd)	250 x 200
Ventral division of the MGB (MGv)	250 x 350
Medial division of the MGB (MGm)	200 x 250
Peripeduncular Nucleus (PP)	530 x 200

1012

1013

Table 2: Statistical analysis of data classified according to CF (<20 kHz vs. ≥20 kHz) are shown for spontaneous activity, minimum threshold (MT) and sound driven activity at MT+15 dB and MT+30 dB.

	CF <20 kHz	**CF>=20 kHz**
	Spontaneous activity	**Spontaneous activity**
Genotype	*F(1,167)=4.274, p=0.04*	*F*(1,333)=0.933, *p*=0.335
Age	*F(2,167)=2.565, p=0.08*	*F*(2,333)=12.938, *p*<0.0001
Genotype-Age Interactions	*F*(2,167)= 4.928, *p*=0.008	*F*(2,333)=0.052, *p*=0.949
	Minimum Threshold	**Minimum Threshold**
Genotype	*F*(1,164)=2.915, *p*=0.09	*F(1,331)=6.436, p*=0.012
Age	*F*(2,164)=13.385, *p*<0.0001	*F(2,331)=12.583, p*<0.0001
Genotype-Age Interactions	*F*(2,164)=1.274, *p*=0.282	*F*(2,331)=1.211, *p*=0.299
	Response Magnitude MT+15 dB	**Response Magnitude MT+15 dB**
Genotype	*F*(1,157)=14.878, *p*=0.00016	*F*(1,316)=0.002, *p*=0.968
Age	*F*(2,157)=1.256, *p*=0.288	*F*(2,316)=6.132, *p*=0.002
Genotype-Age Interactions	*F*(2,157)=0.277, *p*=0.759	*F*(2,316)=1.534, *p*=0.217
	Response Magnitude MT+30 dB	**Response Magnitude MT+30 dB**
Genotype	*F*(1,155)=18.529, *p*=0.000030	*F*(1,314)=0.041, *p*=0.840
Age	*F*(2,155)=1.625, *p*=0.2	*F*(2,314)=5.390, *p*=0.005
Genotype-Age Interactions	*F*(2,155)=2.117, *p*=0.124	*F*(2,314)=5.174, *p*=0.006

Table 3: Statistical analysis of data classified according to CF (<20 kHz vs. ≥20 kHz) are shown for percent turnover, dynamic range and response latency to CF tones presented at MT+15 dB and MT+30 dB.

	CF <20 kHz	**CF>=20 kHz**
	Percent Turnover	**Percent Turnover**
Genotype	*F(1,161)=0.516, p*=0.473	*F(1,330)=4.368, p*=0.037
Age	*F(2,161)=3.624, p*=0.029	*F(2,330)=0.729, p*=0.483
Genotype-Age Interactions	*F*(2,161)=0.405, *p*=0.668	*F*(2,330)=2.704, *p*=0.068
	Dynamic Range	**Dynamic Range**
Genotype	*F(1,127)=0.003, p*=0.959	*F(1,223)=0.011, p*=0.915
Age	*F(2,127)=8.188, p*=0.0004	*F(2,223)=0.053, p*=0.948
Genotype-Age Interactions	*F*(2,127)=2.614, *p*=0.077	*F*(2,223)=1.719, *p*=0.182
	Response Latency at MT+15 dB	**Response Latency at MT+15 dB**
Genotype	*F(1, 163)=4.878, p*=0.029	*F(1,315)=3.430, p*=0.065
Age	*F(2,163)=10.682, p*=0.000044	*F(2,315)=34.024, p*<0.0001
Genotype-Age Interactions	*F*(2,163)=0.297, *p*=0.743	*F*(2,315)=0.130, *p*=0.878
	Response Latency at MT+30 dB	**Response Latency at MT+30 dB**
Genotype	*F(1,143)=4.128, p*=0.044	*F(1,312)=0.253, p*=0.615
Age	*F(2,143)=44.573, p*<0.0001	*F(2,312)=65.186, p*<0.0001
Genotype-Age Interactions	*F*(2,143)=1.405, *p*=0.249	*F*(2,312)=0.045, *p*=0.956

Table 4: Statistical analysis of data classified according to CF (<20 kHz vs. ≥20 kHz). BW10, BW20 and BW30 refer to tuning bandwidth at MT+15 dB, MT+20 dB and MT+30 dB, respectively.

	CF <20 kHz	**CF>=20 kHz**
	BW10	**BW10**
Genotype	$F(1,118)=4.346$, $p=0.039$	$F(1,181)=0.123$, $p=0.726$
Age	$F(2,118)=0.058$, $p=0.944$	$F(2,181)=0.699$, $p=0.499$
Genotype-Age Interactions	$F(2,118)=1.771$, $p=0.175$	$F(2,181)=3.272$, $p=0.04$
	BW20	**BW20**
Genotype	$F(1,118)=5.9$, $p=0.017$	$F(1,182)=1.221$, $p=0.271$
Age	$F(2,118)=0.487$, $p=0.515$	$F(2,182)=2.606$, $p=0.077$
Genotype-Age Interactions	$F(2,118)=0.487$, $p=0.616$	$F(2,182)=0.497$, p=0.609
	BW30	**BW30**
Genotype	$F(1,116)=5.806$, $p=0.018$	$F(1,180)=0.225$, $p=0.636$
Age	$F(2,116)=1.259$, $p=0.288$	$F(2,180)=4.013$, $p=0.20$
Genotype-Age Interactions	$F(2,116)=0.387$, $p=0.68$	$F(2,180)=0.702$, p=0.497

Table 5: Statistical analysis of rate modulation transfer functions (rMTF) obtained from WT and *Fmr1* KO mice at the three developmental time points. The data are organized according to the modulation frequency. 'All' indicates all the neurons combined. CF<20 kHz and CF>=20 kHz indicates when data were split according to CF. *= $p < 0.05$

Modulation Frequency (Hz)	CF Frequency	Genotype x Age Interaction	Main effect of Genotype	Main effect of Age
5	All	F(2,412)=1.973, p=0.140	F(1,412)=2.011, p=0.157	F(2,412)=0.688, p=0.503
	CF<20 kHz	F(2,159)=1.697, p=0.187	F(1,159)=7.366, p=0.007*	F(2,159)=0.832, p=0.437
	CF>=20 kHz	F(2,315)=3.264, P=0.040*	F(2,315)=0.001, p=0.972	F(2,315)=4.279, p=0.015*
10	All	F(2,406)=1.028, p=0.359	F(1,406)=0.573, p=0.450	F(2,406)=1.119, p=0.328
	CF<20 kHz	F(2,159)=1.952, p=0.145	F(2,159)=2.046, p=0.155	F(2,159)=0.337, p=0.715
	CF>=20 kHz	F(2,314)=1.224, p=0.296	F(2,314)=0.641, p=0.424	F(2,314)=2.351, p=0.097
20	All	F(2,415)=0.733, p=0.481	F(1,415)=5.389, p=0.021*	F(2, 415)=4.455, p=0.012*
	CF<20 kHz	F(2,159)=2.732, p=0.068	F(1,159)=5.786, p=0.017*	F(2,159)=1.389, p=0.252
	CF>=20 kHz	F(2,314)=0.334, p=0.717	F(1,314)=2.600, p=0.108	F(2,314)=11.143, p<0.0001*
50	All	F(2,414)=1.538, p=0.216	F(1,414)=16.72, p<0.0001*	F(2,414)=3.378, p=0.035*
	CF<20 kHz	F(2,159)=1.778, p=0.172	F(2,159)=5.013, p=0.027*	F(2,159)=1.008, p=0.367
	CF>=20 kHz	F(2,315)=1.387, p=0.251	F(2,315)=11.473, p=0.001*	F(2,315)=6.064, p=0.003*
100	All	F(2,410)= 2.704,P=0.068	F(1,410)=6.729, P=0.010*	F(2,410)=1.292, P=0.276
	CF<20 kHz	F(2,159)=3.724, p=0.026*	F(2,159)=6.828, p=0.010*	F(2,159)=0.367, p=0.693
	CF>=20 kHz	F(2,293)=2.813, p=0.062	F(1,293)=1.760, p=0.186	F(2,293)=1.599, p=0.204
200	All	F(2,401)=2.282, p=0.103	F(2,401)=1.845, p=0.175	F(2,401)=0.262, p=0.770
	CF<20 kHz	F(2,159)=5.217, p=0.023*	F(2, 159)=5.217, p=0.024*	F(2,159)=0.413, p=0.663
	CF>=20 kHz	F(2,314)=1.709, p=0.183	F(1,314)=0.348, p=0.556	F(2,314)=1.52, p=0.220

Table 6: Statistical analysis of the temporal modulation transfer functions (tMTF) obtained from WT and *Fmr1* KO mice at the three developmental time points. The data are organized according to the modulation frequency. 'All' indicates all the neurons combined. CF<20 kHz and CF>=20 kHz indicates when data were split according to CF. *= $p < 0.05$

Modulation Frequency (Hz)	CF Frequency	Genotype x Age Interaction	Main effect of Genotype	Main effect of Age
5	All CF	F(2,390)=0.127, p=0.881	F(2,390)=2.872, p=0.091	F(2,390)=0.354, p=0.702
	CF<20 kHz	F(2,137)=0.159 p=0.853	F(1,137)=0.472, p=0.493	F(2,137)=0.275, p=0.760
	CF>=20 kHz	F(2,242)=0.052, p=0.949	F(1,242)=2.777, p=0.097	F(2,242)=1.050, p=0.351
10	All CF	F(2,383)=1.989, p=0.138	F(1,383)=4.912, p=0.027*	F(2,383)=2.001, p=0.137
	CF<20 kHz	F(2,136)=0.905, p=0.407	F(1,136)=0.759, p=0.385	F(2,136)=3.110, p=0.048*
	CF>=20 kHz	F(2,235)=1.386, p=0.252	F(1,235)=4.241, p=0.041*	F(2,235)=0.695, p=0.500
20	All CF	F(2,387)=2.353, p=0.096	F(2,387)=1.702, p=0.193	F(2,387)=4.997, p=0.007*
	CF<20 kHz	F(2,135)=0.887, p=0.414	F(1,135)=1.069, p=0.303	F(2,135)=3.287, p=0.040*
	CF>=20 kHz	F(2,240)=2.087, p=0.126	F(1,240)=0.599, p=0.440	F(2,240)=1.734, p=0.179
50	All CF	F(2,382)=2.058, p=0.129	F(1,382)=0.752, p=0.386	F(2,382)=0.609, p=0.544
	CF<20 kHz	F(2,129)=0.918, p=0.402	F(1,129)=0.226, p=0.636	F(2,129)=0.836, p=0.436
	CF>=20 kHz	F(2,241)=0.819, p=0.442	F(1,241)=0.08, p=0.778	F(2,241)=1.173, p=0.311
100	All CF	F(2,388)=0.153, p=0.858	F(1,388)=0.061, p=0.804	F(2,388)=22.195, p<0.0001*
	CF<20 kHz	F(2,130)=0.502, p=0.607	F(1,130)=1.124, p=0.291	F(2,130)=8.009, p=0.001
	CF>=20 kHz	F(2,248)=0.356, p=0.701	F(1,248)=0.119, p=0.731	F(2,248)=12.587, p<0.0001*
200	All CF	F(2,352)=1.356, p=0.259	F(1,352)=0.932, p=0.335	F(2,352)=9.349, p=0.0001*
	CF<20 kHz	F(2,120)=0.433, p=0.650	F(2,120)=0.027, p=0.870	F(2,120)=4.008, p=0.021*
	CF>=20 kHz	F(2,222)=1.738, p=0.178	F(1,222)1.245, p=0.266	F(2,222)=4.665)=0.010*

References

Antoine, M.W., Langberg, T., Schnepel, P. and Feldman, D.E., 2019. Increased excitation-inhibition ratio stabilizes synapse and circuit excitability in four autism mouse models. *Neuron*, *101*(4), pp.648-661.

Aitkin, L.M. and Moore, D.R., 1975. Inferior colliculus. II. Development of tuning characteristics and tonotopic organization in central nucleus of the neonatal cat. *Journal of neurophysiology*, *38*(5), pp.1208-1216.

Arnault, P., and Roger, M. (1987). The connection of the peripeduncular area studied by retrograde and anterograde transport in the rat. J. Comp. Neurol. *258*, 463–476.

Bakker, C.E., and Oostra, B.A. (2003). Understanding fragile X syndrome: insights from animal models. Cytogenet. Genome Res. *100*, 111–123.

Beebe, K., Wang, Y., and Kulesza, R. (2014). Distribution of fragile X mental retardation protein in the human auditory brainstem. Neuroscience *273*, 79–91.

Brown, M.R., Kronengold, J., Gazula, V.-R., Chen, Y., Strumbos, J.G., Sigworth, F.J., Navaratnam, D., and Kaczmarek, L.K. (2010). Fragile X mental retardation protein controls gating of the sodium-activated potassium channel Slack. Nat. Neurosci. *13*, 819–821.

Bülow, P., Murphy, T.J., Bassell, G.J. and Wenner, P., 2019. Homeostatic Intrinsic Plasticity Is Functionally Altered in Fmr1 KO Cortical Neurons. *Cell reports*, *26*(6), pp.1378-1388.

Castrén, M., Pääkkönen, A., Tarkka, I.M., Ryynänen, M., and Partanen, J. (2003). Augmentation of Auditory N1 in Children with Fragile X Syndrome. Brain Topogr. *15*, 165–171.

Chen, L., and Toth, M. (2001). Fragile X mice develop sensory hyperreactivity to auditory stimuli. Neuroscience *103*, 1043–1050.

Cho, J.-H., Bayazitov, I.T., Meloni, E.G., Myers, K.M., Carlezon, W.A., Zakharenko, S.S., and Bolshakov, V.Y. (2011). Coactivation of Thalamic and Cortical Pathways Induces Input Timing-Dependent Plasticity in Amygdala. Nat. Neurosci. *15*, 113–122.

Choy Buentello, D., Bishop, D.C., and Oliver, D.L. (2015). Differential distribution of GABA and glycine terminals in the inferior colliculus of rat and mouse. J. Comp. Neurol. *523*, 2683–2697.

Cramer, K.S., and Gabriele, M.L. (2014). Axon guidance in the auditory system: multiple functions of Eph receptors. Neuroscience *277*, 152–162.

Curia, G., Papouin, T., Séguéla, P., and Avoli, M. (2009). Downregulation of tonic GABAergic inhibition in a mouse model of fragile X syndrome. Cereb. Cortex N. Y. N 1991 *19*, 1515–1520.

Dansie, L.E., Phommahaxay, K., Okusanya, A.G., Uwadia, J., Huang, M., Rotschafer, S.E., Razak, K.A., Ethell, D.W. and Ethell, I.M., 2013. Long-lasting effects of minocycline on behavior in young but not adult Fragile X mice. *Neuroscience*, *246*, pp.186-198.

D'Hulst, C., De Geest, N., Reeve, S.P., Van Dam, D., De Deyn, P.P., Hassan, B.A., and Kooy, R.F. (2006). Decreased expression of the GABAA receptor in fragile X syndrome. Brain Res. *1121*, 238–245.

Dölen, G., Osterweil, E., Rao, B.S.S., Smith, G.B., Auerbach, B.D., Chattarji, S., and Bear, M.F. (2007). Correction of Fragile X Syndrome in Mice. Neuron *56*, 955–962.

Ehret, G. and Romand, R., 1992. Development of tone response thresholds, latencies and tuning in the mouse inferior colliculus. *Developmental brain research*, *67*(2), pp.317-326.

Ethridge, L.E., White, S.P., Mosconi, M.W., Wang, J., Byerly, M.J., and Sweeney, J.A. (2016). Reduced habituation of auditory evoked potentials indicate cortical hyper-excitability in Fragile X Syndrome. Transl. Psychiatry *6*, e787.

Ethridge, L.E., White, S.P., Mosconi, M.W., Wang, J., Pedapati, E.V., Erickson, C.A., Byerly, M.J., and Sweeney, J.A. (2017). Neural synchronization deficits linked to cortical hyper-excitability and auditory hypersensitivity in fragile X syndrome. Mol. Autism *8*, 22.

Faingold, C.L. (2002). Role of GABA abnormalities in the inferior colliculus pathophysiology – audiogenic seizures. Hear. Res. *168*, 223–237.

Faingold, C.L., and Boersma Anderson, C.A. (1991). Loss of intensity-induced inhibition in inferior colliculus neurons leads to audiogenic seizure susceptibility in behaving genetically epilepsy-prone rats. Exp. Neurol. *113*, 354–363.

Faingold, C.L., Anderson, C.A.B. and Caspary, D.M., 1991. Involvement of GABA in acoustically-evoked inhibition in inferior colliculus neurons. *Hearing research*, *52*(1), pp.201-216.

Fathke, R.L. and Gabriele, M.L., 2009. Patterning of multiple layered projections to the auditory midbrain prior to experience. *Hearing research*, *249*(1-2), pp.36-43.

Faingold, C.L., and Randall, M.E. (1999). Neurons in the deep layers of superior colliculus play a critical role in the neuronal network for audiogenic seizures: mechanisms for production of wild running behavior. Brain Res. *815*, 250–258.

Felix, R.A., and Portfors, C.V. (2007). Excitatory, inhibitory and facilitatory frequency response areas in the inferior colliculus of hearing impaired mice. Hear. Res. *228*, 212–229.

Frankland, P.W., Wang, Y., Rosner, B., Shimizu, T., Balleine, B.W., Dykens, E.M., Ornitz, E.M., and Silva, A.J. (2004). Sensorimotor gating abnormalities in young males with fragile X syndrome and Fmr1-knockout mice. Mol. Psychiatry *9*, 417–425.

Fulop, D.B., Humli, V., Szepesy, J., Ott, V., Reglodi, D., Gaszner, B., Nemeth, A., Szirmai, A., Tamas, L., Hashimoto, H. and Zelles, T., 2019. Hearing impairment and associated morphological changes in pituitary adenylate cyclase activating polypeptide (PACAP)-deficient mice. *Scientific reports*, *9*(1), pp.1-15.

Fuzessery, Z.M. and Hall, J.C., 1996. Role of GABA in shaping frequency tuning and creating FM sweep selectivity in the inferior colliculus. *Journal of neurophysiology*, *76*(2), pp.1059-1073.

Gabriele, M.L., Brunso-Bechtold, J.K. and Henkel, C.K., 2000a. Plasticity in the development of afferent patterns in the inferior colliculus of the rat after unilateral cochlear ablation. *Journal of Neuroscience*, *20*(18), pp.6939-6949.

Gabriele, M.L., Brunso-Bechtold, J.K. and Henkel, C.K., 2000b. Development of afferent patterns in the inferior colliculus of the rat: projection from the dorsal nucleus of the lateral lemniscus. *Journal of Comparative Neurology*, *416*(3), pp.368-382.

Garcia-Pino, E., Gessele, N., and Koch, U. (2017). Enhanced Excitatory Connectivity and Disturbed Sound Processing in the Auditory Brainstem of Fragile X Mice. J. Neurosci. *37*, 7403–7419.

Goldberg, J.M., and Brown, P.B. (1969). Response of binaural neurons of dog superior olivary complex to dichotic tonal stimuli: some physiological mechanisms of sound localization. J. Neurophysiol. *32*, 613–636.

Grimsley, C.A., Sanchez, J. and Sivaramakrishnan, S., 2013. Midbrain local circuits shape sound intensity codes. *Frontiers in neural circuits*, *7*, p.174.

Henkel, C.K., Keiger, C.J., Franklin, S.R. and Brunso-Bechtold, J.K., 2007. Development of banded afferent compartments in the inferior colliculus before onset of hearing in ferrets. *Neuroscience*, *146*(1), pp.225-235.

Hitoglou, M., Ververi, A., Antoniadis, A., and Zafeiriou, D.I. (2010). Childhood Autism and Auditory System Abnormalities. Pediatr. Neurol. *42*, 309–314.

Howorth, P.W., Teschemacher, A.G. and Pickering, A.E., 2009. Retrograde adenoviral vector targeting of nociresponsive pontospinal noradrenergic neurons in the rat in vivo. *Journal of Comparative Neurology*, *512*(2), pp.141-157.

Hurley, L.M., Tracy, J.A. and Bohorquez, A., 2008. Serotonin 1B receptor modulates frequency response curves and spectral integration in the inferior colliculus by reducing GABAergic inhibition. *Journal of neurophysiology*, *100*(3), pp.1656-1667.

Kazdoba, T.M., Leach, P.T., Silverman, J.L., and Crawley, J.N. (2014). Modeling fragile X syndrome in the Fmr1 knockout mouse. Intractable Rare Dis. Res. *3*, 118–133.

Kokash, J., Alderson, E.M., Reinhard, S.M., Crawford, C.A., Binder, D.K., Ethell, I.M., and Razak, K.A. (2019). Genetic reduction of MMP-9 in the Fmr1 KO mouse partially rescues prepulse inhibition of acoustic startle response. Brain Res. *1719*, 24–29.

Kulinich AO, Reinhard SM, Rais M, Lovelace JW, Scott V, Binder DK, Razak KA, Ethell IM. 2020. Beneficial effects of sound exposure on auditory cortex development in a mouse model of Fragile X Syndrome. Neurobiology of Disease.134: 104622.

Le Beau, F.E., Rees, A.D.R.I.A.N. and Malmierca, M.S., 1996. Contribution of GABA- and glycine-mediated inhibition to the monaural temporal response properties of neurons in the inferior colliculus. *Journal of neurophysiology*, *75*(2), pp.902-919.

LeDoux, J.E., Farb, C.R., and Milner, T.A. (1991). Ultrastructure and synaptic associations of auditory thalamo-amygdala projections in the rat. Exp. Brain Res. *85*, 577–586.

Lovelace, J.W., Wen, T.H., Reinhard, S., Hsu, M.S., Sidhu, H., Ethell, I.M., Binder, D.K., and Razak, K.A. (2016). Matrix metalloproteinase-9 deletion rescues auditory evoked potential habituation deficit in a mouse model of Fragile X Syndrome. Neurobiol. Dis. *89*, 126–135.

Lovelace, J.W., Ethell, I.M., Binder, D.K., and Razak, K.A. (2018). Translation-relevant EEG phenotypes in a mouse model of Fragile X Syndrome. Neurobiol. Dis. *115*, 39–48.

Lovelace, J.W., Rais, M., Palacios, A.R., Shuai, X.S., Bishay, S., Popa, O., Pirbhoy, P.S., Binder, D.K., Nelson, D.L., Ethell, I.M., et al (2019). Deletion of Fmr1 from Forebrain Excitatory Neurons Triggers Abnormal Cellular, EEG, and Behavioral Phenotypes in the Auditory Cortex of a Mouse Model of Fragile X Syndrome. Cereb. Cortex.

Martin del Campo, H.N., Measor, K.R., and Razak, K.A. (2012). Parvalbumin immunoreactivity in the auditory cortex of a mouse model of presbycusis. Hear. Res. *294*, 31–39.

Merchán, M., Aguilar, L.A., Lopez-Poveda, E.A., and Malmierca, M.S. (2005). The inferior colliculus of the rat: quantitative immunocytochemical study of GABA and glycine. Neuroscience *136*, 907–925.

McCullagh EA, Rotschafer SE, Auerbach BD, Klug A, Kaczmarek LK, Cramer KS, Kulesza RJ Jr., Razak KA, Lovelace JW, Lu Y, Koch U, Wang Y. Mechanisms

Underlying Auditory Hypersensitivity in Fragile X Syndrome. The FASEB Journal, *In Press.*

Meredith, R.M., Dawitz, J. and Kramvis, I., 2012. Sensitive time-windows for susceptibility in neurodevelopmental disorders. *Trends in neurosciences*, *35*(6), pp.335-344.

Michalon, A., Sidorov, M., Ballard, T.M., Ozmen, L., Spooren, W., Wettstein, J.G., Jaeschke, G., Bear, M.F., and Lindemann, L. (2012). Chronic Pharmacological mGlu5 Inhibition Corrects Fragile X in Adult Mice. Neuron *74*, 49–56.

Millan, M.H., Meldrum, B.S., and Faingold, C.L. (1986). Induction of audiogenic seizure susceptibility by focal infusion of excitant amino acid or bicuculline into the inferior colliculus of normal rats. Exp. Neurol. *91*, 634–639.

Miller, L.J., McIntosh, D.N., McGrath, J., Shyu, V., Lampe, M., Taylor, A.K., Tassone, F., Neitzel, K., Stackhouse, T., and Hagerman, R.J. (1999). Electrodermal responses to sensory stimuli in individuals with fragile X syndrome: a preliminary report. Am. J. Med. Genet. *83*, 268–279.

Musumeci, S.A., Bosco, P., Calabrese, G., Bakker, C., De Sarro, G.B., Elia, M., Ferri, R., and Oostra, B.A. (2000). Audiogenic seizures susceptibility in transgenic mice with fragile X syndrome. Epilepsia *41*, 19–23.

Musumeci, S.A., Calabrese, G., Bonaccorso, C.M., D'Antoni, S., Brouwer, J.R., Bakker, C.E., Elia, M., Ferri, R., Nelson, D.L., Oostra, B.A., et al. (2007). Audiogenic seizure susceptibility is reduced in fragile X knockout mice after introduction of FMR1 transgenes. Exp. Neurol. *203*, 233–240.

Numa, C., Nagai, H., Taniguchi, M., Nagai, M., Shinohara, R. and Furuyashiki, T., 2019. Social defeat stress-specific increase in c-Fos expression in the extended amygdala in mice: Involvement of dopamine D1 receptor in the medial prefrontal cortex. *Scientific reports*, *9*(1), pp.1-9.

Oswald, A.-M.M., and Reyes, A.D. (2008). Maturation of intrinsic and synaptic properties of layer 2/3 pyramidal neurons in mouse auditory cortex. J. Neurophysiol. *99*, 2998–3008.

Oswald, A.-M.M., and Reyes, A.D. (2011). Development of Inhibitory Timescales in Auditory Cortex. Cereb. Cortex N. Y. NY *21*, 1351–1361.

Pacey, L.K.K., Heximer, S.P., and Hampson, D.R. (2009). Increased GABAB Receptor-Mediated Signaling Reduces the Susceptibility of Fragile X Knockout Mice to Audiogenic Seizures. Mol. Pharmacol. *76*, 18–24.

Palombi, P.S., and Caspary, D.M. (1996). GABA inputs control discharge rate primarily within frequency receptive fields of inferior colliculus neurons. J. Neurophysiol. *75*, 2211–2219.

Phillips, D.P., and Kelly, J.B. (1989). Coding of tone-pulse amplitude by single neurons in auditory cortex of albino rats (Rattus norvegicus). Hear. Res. *37*, 269–279.

Preibisch, S., Saalfeld, S., and Tomancak, P. (2009). Globally optimal stitching of tiled 3D microscopic image acquisitions. Bioinformatics *25*, 1463–1465.

Rais, M., Binder, D.K., Razak, K.A., and Ethell, I.M. (2018). Sensory Processing Phenotypes in Fragile X Syndrome. ASN Neuro *10*, 1759091418801092.

Razak KA, Dominick K and Erickson, CA. Developmental studies in Fragile X Syndrome. J Neurodev. Disorders. *In Press*.

Reinhard, S.M., Rais, M., Afroz, S., Hanania, Y., Pendi, K., Espinoza, K., Rosenthal, R., Binder, D.K., Ethell, I.M., and Razak, K.A. (2019). Reduced perineuronal net expression in Fmr1 KO mice auditory cortex and amygdala is linked to impaired fear-associated memory. Neurobiol. Learn. Mem. *164*, 107042.

Rogers, S.J., Hepburn, S., and Wehner, E. (2003). Parent reports of sensory symptoms in toddlers with autism and those with other developmental disorders. J. Autism Dev. Disord. *33*, 631–642.

Romand, R., and Ehret, G. (1990). development of tonotopy in the inferior colliculus. I. Electrophysiological mapping in house mice. Dev. Brain Res. *54*, 221–234.

Rotschafer, S., and Razak, K. (2013). Altered auditory processing in a mouse model of fragile X syndrome. Brain Res. *1506*, 12–24.

Rotschafer, S.E., and Cramer, K.S. (2017). Developmental Emergence of Phenotypes in the Auditory Brainstem Nuclei of Fmr1 Knockout Mice. ENeuro *4*, ENEURO.0264-17.2017.

Rotschafer, S.E., Marshak, S., and Cramer, K.S. (2015). Deletion of Fmr1 Alters Function and Synaptic Inputs in the Auditory Brainstem. PLoS ONE *10*.

Ruby, K., Falvey, K., and Kulesza, R.J. (2015). Abnormal neuronal morphology and neurochemistry in the auditory brainstem of Fmr1 knockout rats. Neuroscience *303*, 285–298.

Sanes, D.H., Geary, W.A., Wooten, G.F., and Rubel, E.W. (1987). Quantitative distribution of the glycine receptor in the auditory brain stem of the gerbil. J. Neurosci. *7*, 3793–3802.

Schneider, A., Leigh, M.J., Adams, P., Nanakul, R., Chechi, T., Olichney, J., Hagerman, R., and Hessl, D. (2013). Electrocortical changes associated with minocycline treatment in fragile X syndrome. J. Psychopharmacol. (Oxf.) *27*, 956–963.

Shnerson, A. and Willott, J.F., 1979. Development of inferior colliculus response properties in C57BL/6J mouse pups. *Experimental brain research*, *37*(2), pp.373-385.

Smith, L.E., Barker, E.T., Seltzer, M.M., Abbeduto, L., and Greenberg, J.S. (2012). Behavioral Phenotype of Fragile X Syndrome in Adolescence and Adulthood. Am. J. Intellect. Dev. Disabil. *117*, 1–17.

Strumbos, J.G., Brown, M.R., Kronengold, J., Polley, D.B., and Kaczmarek, L.K. (2010). Fragile X mental retardation protein is required for rapid experience-dependent regulation of the potassium channel Kv3.1b. J. Neurosci. Off. J. Soc. Neurosci. *30*, 10263–10271.

Sturm, J., Nguyen, T. and Kandler, K., 2014. Development of intrinsic connectivity in the central nucleus of the mouse inferior colliculus. *Journal of Neuroscience*, *34*(45), pp.15032-15046.

Vislay, R.L., Martin, B.S., Olmos-Serrano, J.L., Kratovac, S., Nelson, D.L., Corbin, J.G. and Huntsman, M.M., 2013. Homeostatic responses fail to correct defective amygdala inhibitory circuit maturation in fragile X syndrome. *Journal of Neuroscience*, *33*(17), pp.7548-7558.

Wang, J., Ethridge, L.E., Mosconi, M.W., White, S.P., Binder, D.K., Pedapati, E.V., Erickson, C.A., Byerly, M.J., and Sweeney, J.A. (2017). A resting EEG study of neocortical hyperexcitability and altered functional connectivity in fragile X syndrome. J. Neurodev. Disord. *9*, 11.

Wang, Y., Sakano, H., Beebe, K., Brown, M.R., de Laat, R., Bothwell, M., Kulesza, R.J., and Rubel, E.W. (2014). Intense and specialized dendritic localization of the fragile X mental retardation protein in binaural brainstem neurons: A comparative study in the alligator, chicken, gerbil, and human. J. Comp. Neurol. *522*, 2107–2128.

Wen, T.H., Afroz, S., Reinhard, S.M., Palacios, A.R., Tapia, K., Binder, D.K., Razak, K.A., and Ethell, I.M. (2018). Genetic Reduction of Matrix Metalloproteinase-9 Promotes Formation of Perineuronal Nets Around Parvalbumin-Expressing Interneurons and Normalizes Auditory Cortex Responses in Developing Fmr1 Knock-Out Mice. Cereb. Cortex *28*, 3951–3964.

Wen, T.H., Lovelace, J.W., Ethell, I.M., Binder, D.K. and Razak, K.A., 2019. Developmental changes in EEG phenotypes in a mouse model of fragile X syndrome. *Neuroscience*, *398*, pp.126-143.

Yan, Q.J., Rammal, M., Tranfaglia, M., and Bauchwitz, R.P. (2005). Suppression of two major Fragile X Syndrome mouse model phenotypes by the mGluR5 antagonist MPEP. Neuropharmacology *49*, 1053–1066.

Yang Y, Lee J, Kim G. Integration of locomotion and auditory signals in the mouse inferior colliculus. eLife, In Press. pii: e52228. doi: 10.7554/eLife.52228.

Zhang, H. and Kelly, J.B., 2003. Glutamatergic and GABAergic regulation of neural responses in inferior colliculus to amplitude-modulated sounds. *Journal of neurophysiology*, *90*(1), pp.477-490.

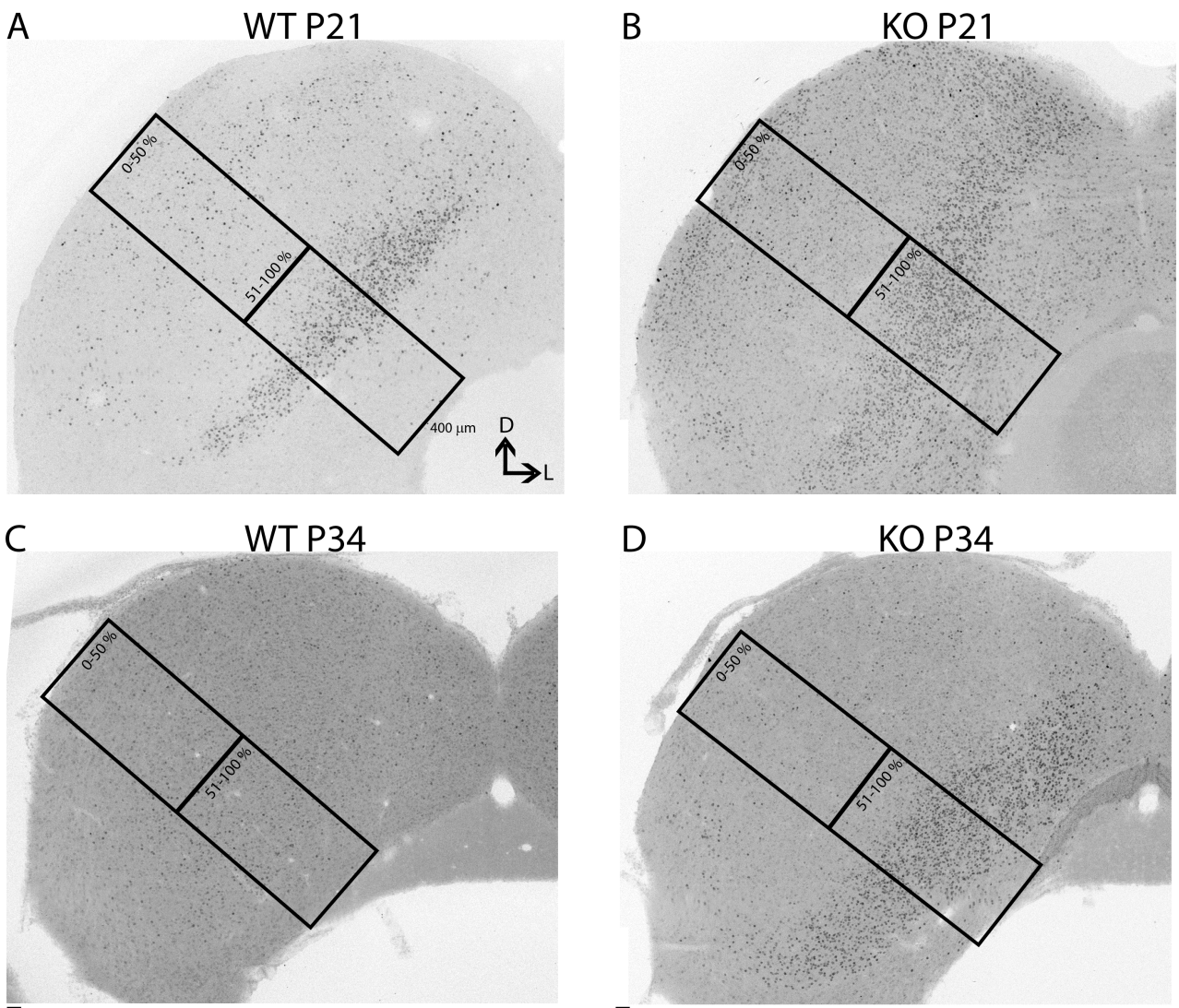
A
WT P21
0-50 %
51-100 %
400 µm
D
L
B
KO P21
0-50 %
51-100 %
C
WT P34
0-50 %
51-100 %
D
KO P34
0-50 %
51-100 %

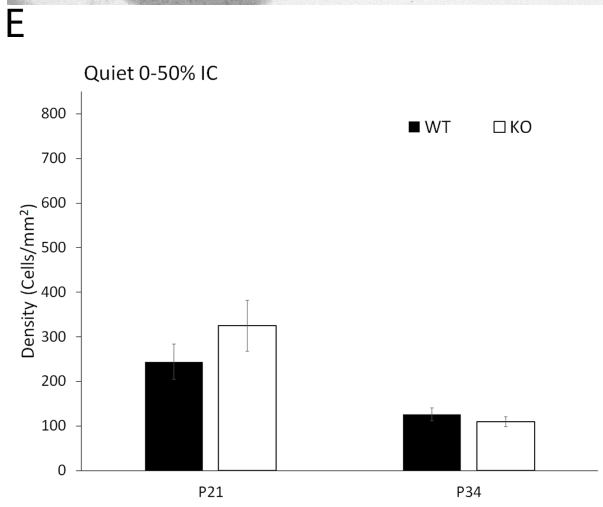
E
Quiet 0-50% IC
WT
KO
Density (Cells/mm²)
800
700
600
500
400
300
200
100
0
P21
P34

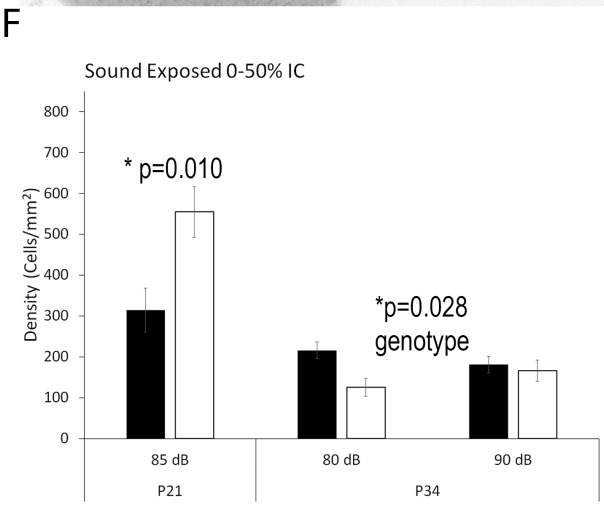
F
Sound Exposed 0-50% IC
Density (Cells/mm²)
* p=0.010
*p=0.028
genotype
800
700
600
500
400
300
200
100
0
85 dB
80 dB
90 dB
P21
P34

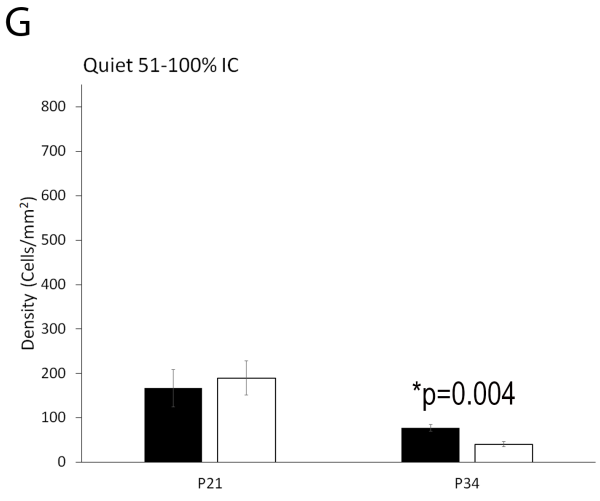
G
Quiet 51-100% IC
Density (Cells/mm²)
*p=0.004
800
700
600
500
400
300
200
100
0
P21
P34

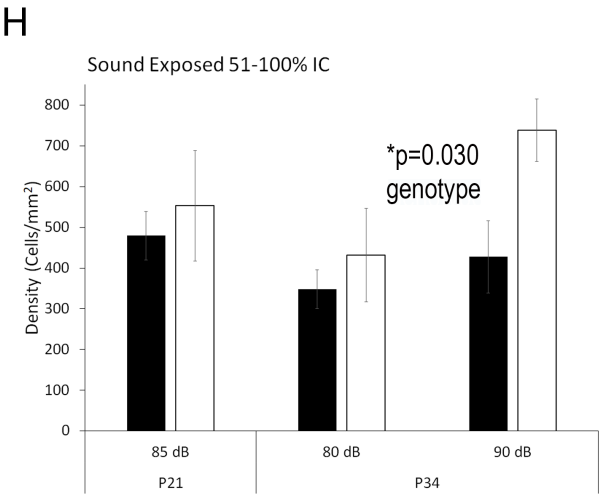
H
Sound Exposed 51-100% IC
Density (Cells/mm²)
*p=0.030
genotype
800
700
600
500
400
300
200
100
0
85 dB
80 dB
90 dB
P21
P34

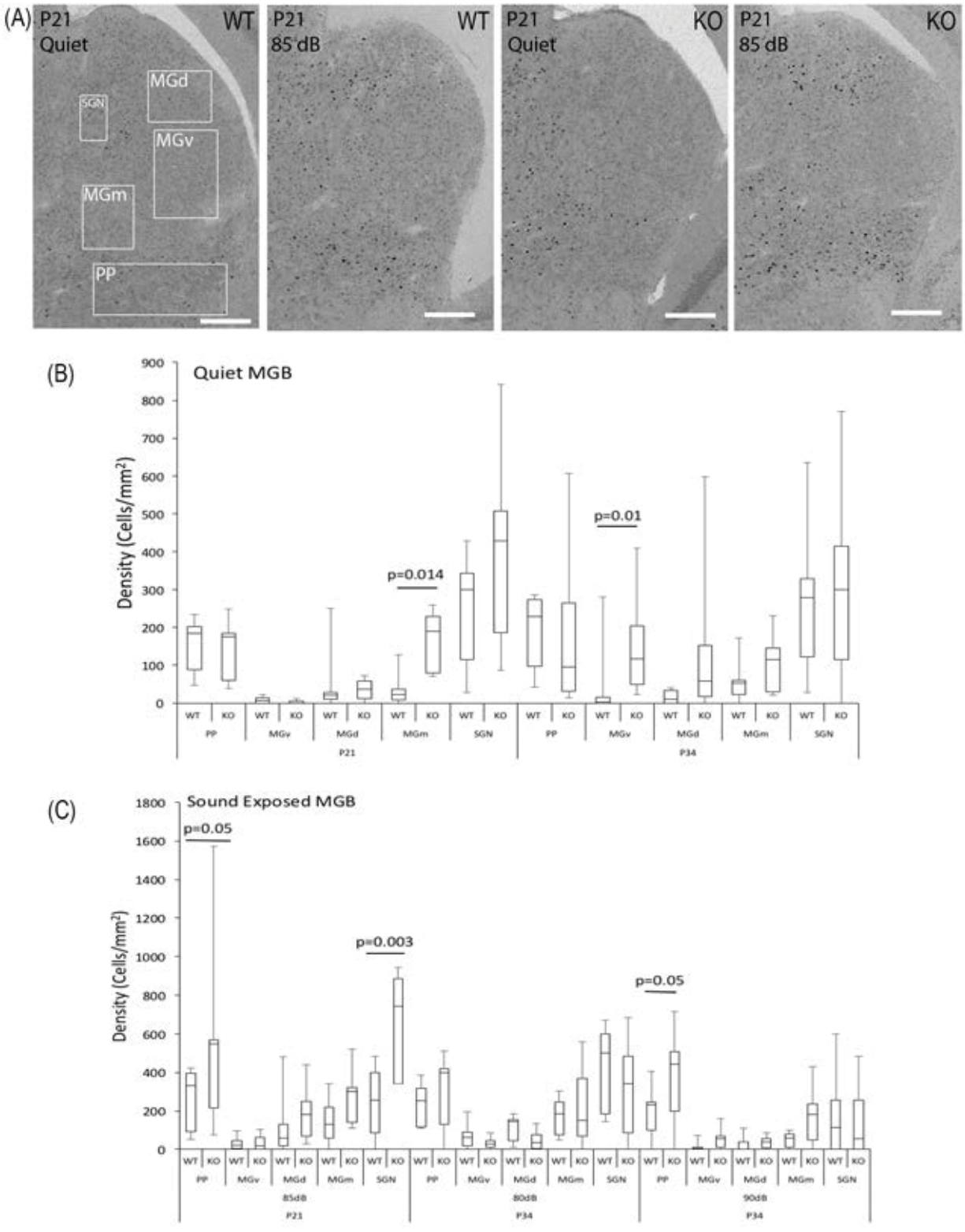
(A)
P21
Quiet
WT
MGd
SGN
MGv
MGm
PP
P21
85 dB
WT
P21
Quiet
KO
P21
85 dB
KO
(B)
Quiet MGB
Density (Cells/mm²)
900
800
700
600
500
400
300
200
100
0
p=0.014
p=0.01
WT KO WT KO WT KO WT KO WT KO WT KO WT KO WT KO WT KO WT KO
PP MGv MGd MGm SGN PP MGv MGd MGm SGN
P21 P34
(C)
Sound Exposed MGB
Density (Cells/mm²)
1800
1600
1400
1200
1000
800
600
400
200
0
p=0.05
p=0.003
p=0.05
WT KO WT KO WT KO WT KO WT KO WT KO WT KO WT KO WT KO WT KO WT KO WT KO WT KO WT KO WT KO WT KO
PP MGv MGd MGm SGN PP MGv MGd MGm SGN PP MGv MGd MGm SGN
85dB 80dB 90dB
P21 P34 P34

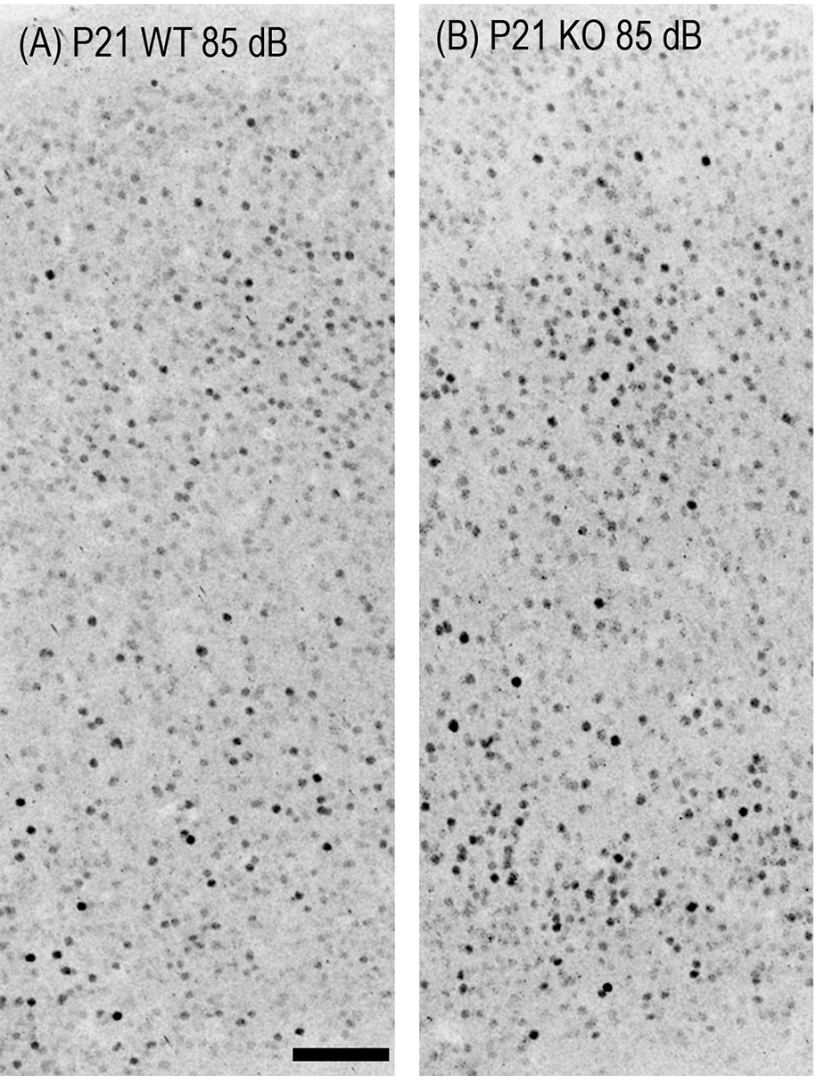
(A) P21 WT 85 dB
(B) P21 KO 85 dB

(C)

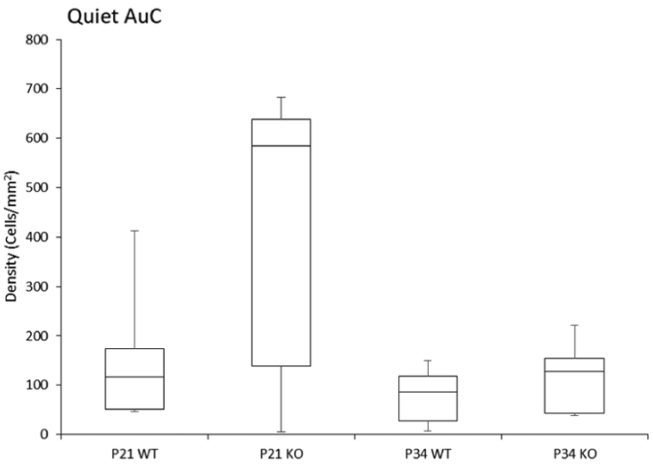
Quiet AuC
Density (Cells/mm²)
800
700
600
500
400
300
200
100
0
P21 WT
P21 KO
P34 WT
P34 KO

(D)

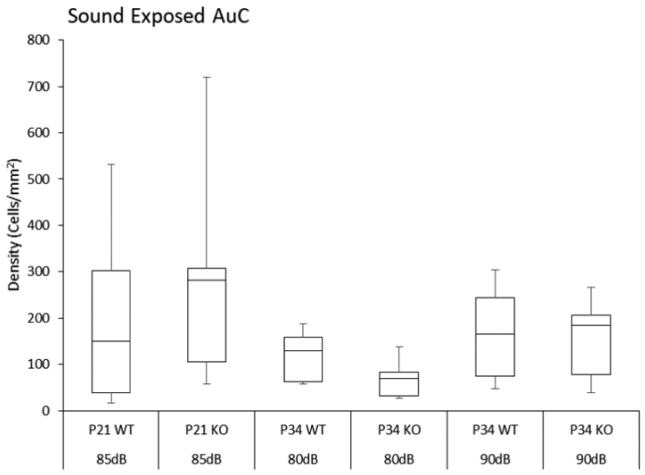
Sound Exposed AuC
Density (Cells/mm²)
800
700
600
500
400
300
200
100
0
P21 WT 85dB
P21 KO 85dB
P34 WT 80dB
P34 KO 80dB
P34 WT 90dB
P34 KO 90dB

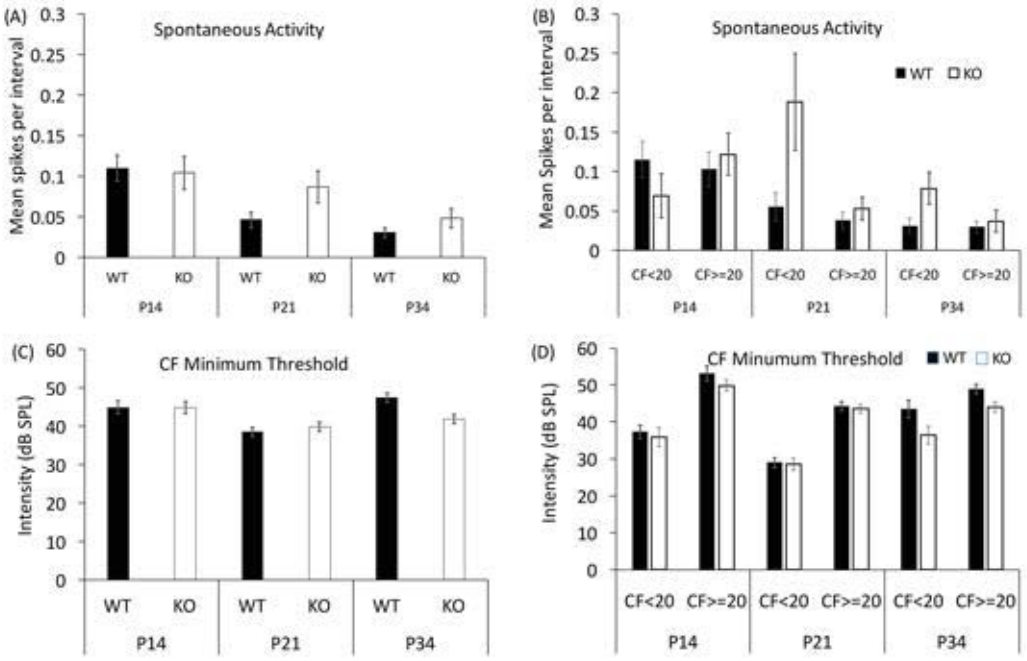
(A)
Spontaneous Activity
Mean spikes per interval
0.3
0.25
0.2
0.15
0.1
0.05
0
WT
KO
P14
P21
P34
(B)
Spontaneous Activity
WT
KO
Mean Spikes per interval
CF<20
CF>=20
(C)
CF Minimum Threshold
Intensity (dB SPL)
60
50
40
30
20
10
(D)
CF Minumum Threshold

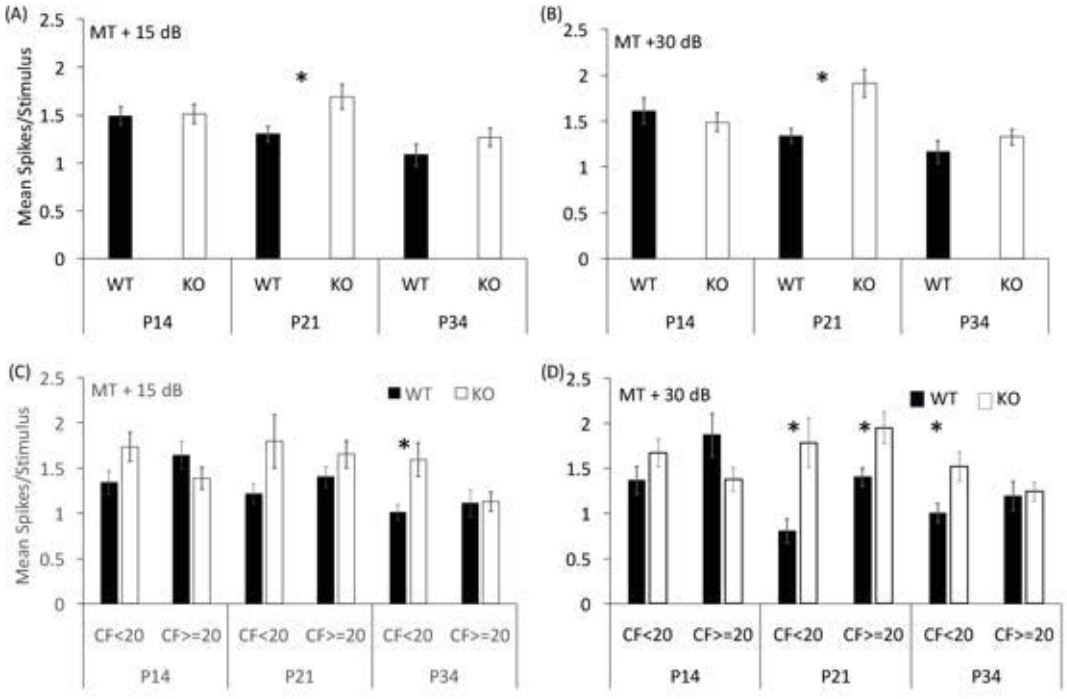
(A)
MT + 15 dB
Mean Spikes/Stimulus
2.5
2
1.5
1
0.5
0
WT
KO
P14
P21
P34
(B)
MT +30 dB
(C)
MT + 15 dB
WT
KO
CF<20
CF>=20
(D)
MT + 30 dB

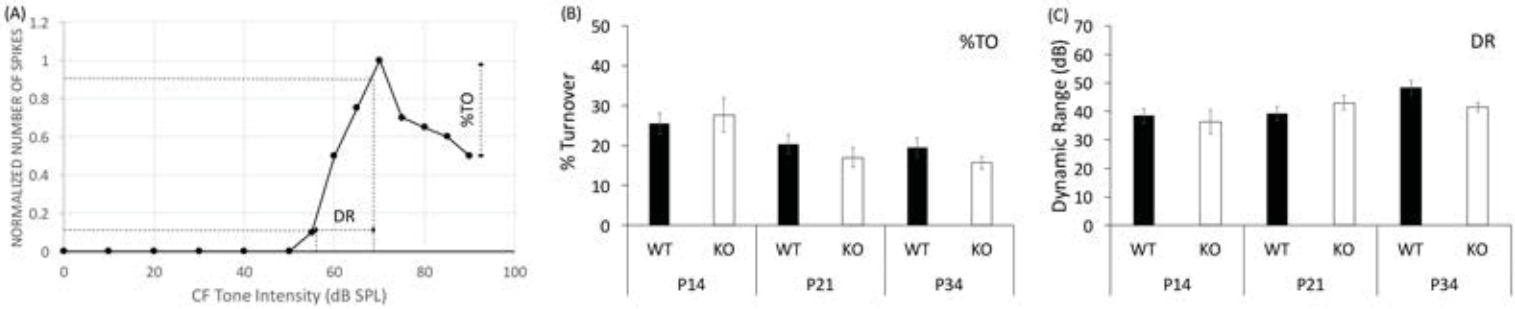
(A)
NORMALIZED NUMBER OF SPIKES
1.2
1
0.8
0.6
0.4
0.2
0
0
20
40
60
80
100
CF Tone Intensity (dB SPL)
DR
%TO
(B)
% Turnover
50
40
30
20
10
0
%TO
WT
KO
WT
KO
WT
KO
P14
P21
P34
(C)
Dynamic Range (dB)
70
60
50
40
30
20
10
0
DR
WT
KO
WT
KO
WT
KO
P14
P21
P34

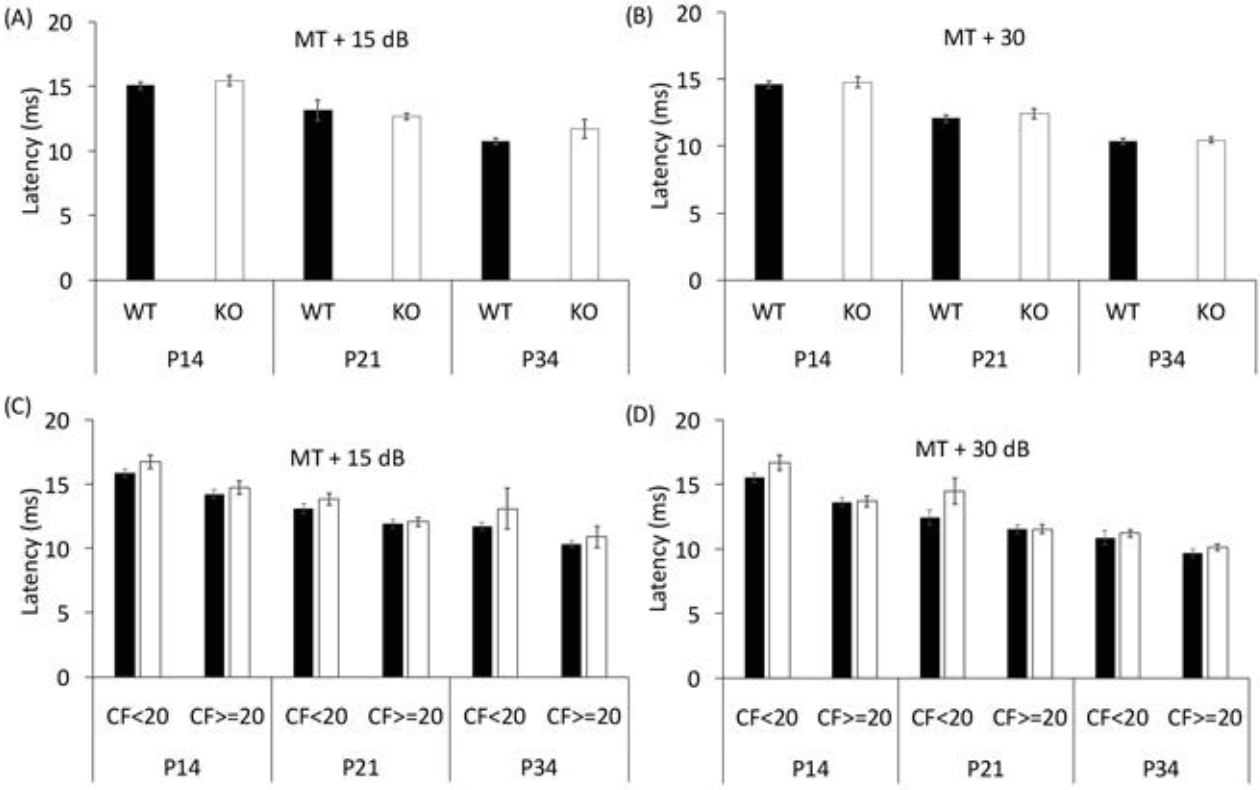
(A)
MT + 15 dB
Latency (ms)
20
15
10
5
0
WT
KO
P14
P21
P34
(B)
MT + 30
(C)
MT + 15 dB
CF<20
CF>=20
(D)
MT + 30 dB

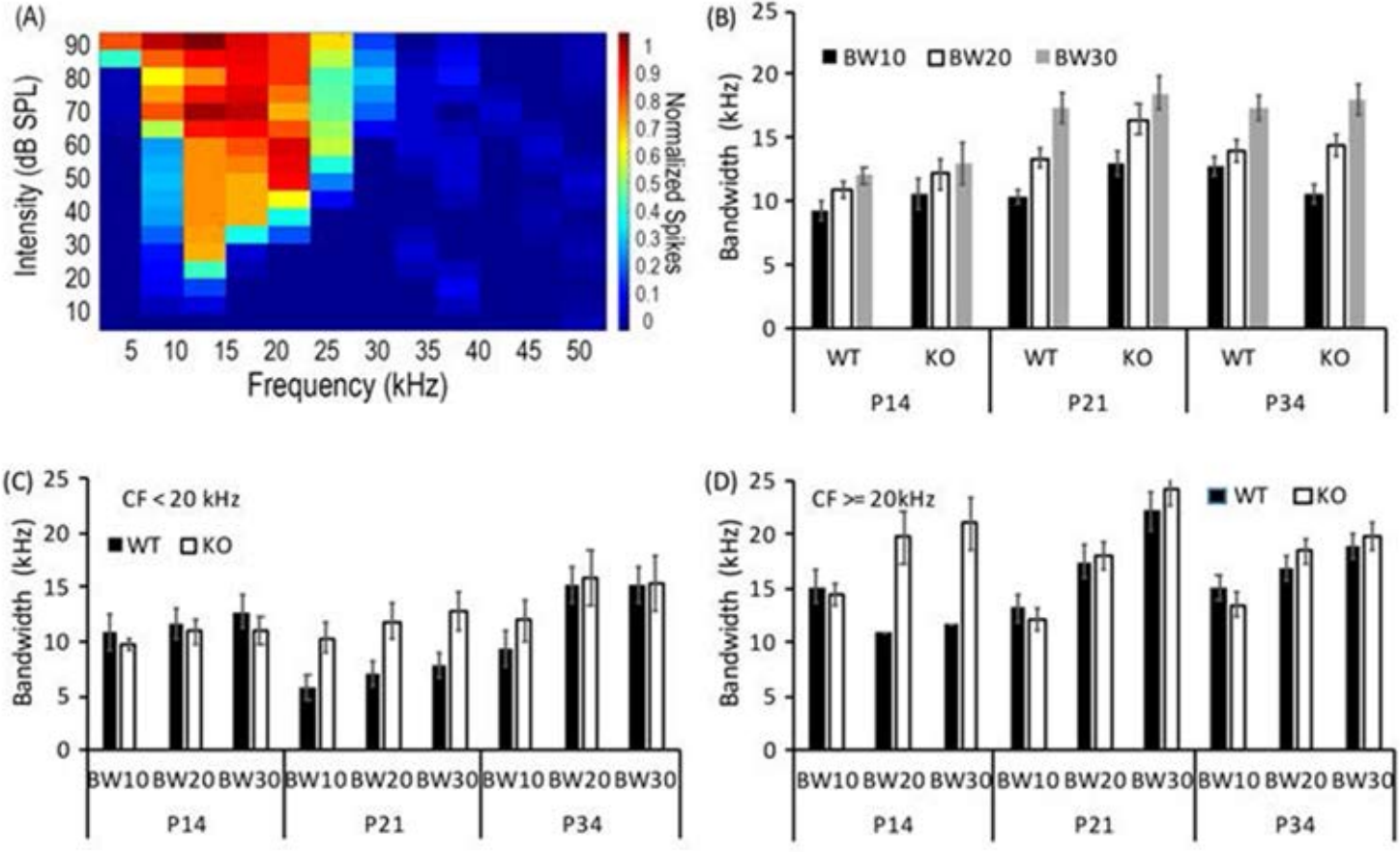
(A)
Intensity (dB SPL)
90
80
70
60
50
40
30
20
10
5 10 15 20 25 30 35 40 45 50
Frequency (kHz)
Normalized Spikes
1
0.9
0.8
0.7
0.6
0.5
0.4
0.3
0.2
0.1
0
(B)
BW10 BW20 BW30
Bandwidth (kHz)
25
20
15
10
5
0
WT KO WT KO WT KO
P14 P21 P34
(C)
CF < 20 kHz
WT KO
Bandwidth (kHz)
BW10 BW20 BW30 BW10 BW20 BW30 BW10 BW20 BW30
P14 P21 P34
(D)
CF >= 20kHz
WT KO
Bandwidth (kHz)
BW10 BW20 BW30 BW10 BW20 BW30 BW10 BW20 BW30
P14 P21 P34

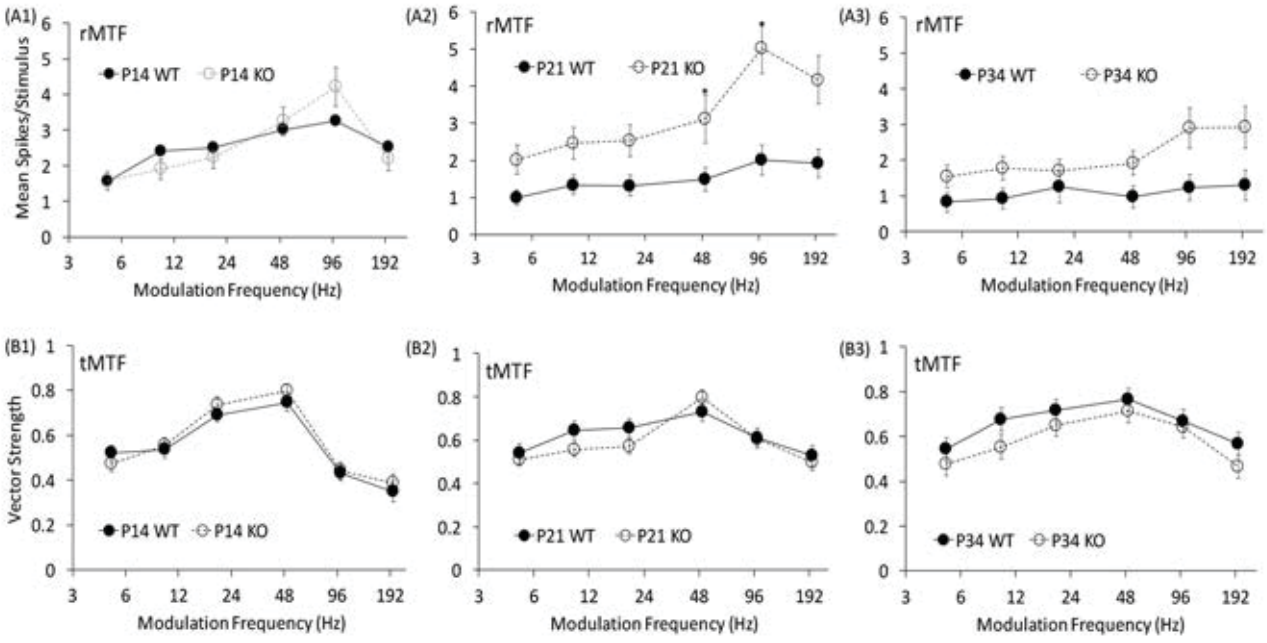
(A1)
rMTF
Mean Spikes/Stimulus
P14 WT
P14 KO
Modulation Frequency (Hz)
(A2)
rMTF
P21 WT
P21 KO
Modulation Frequency (Hz)
(A3)
rMTF
P34 WT
P34 KO
Modulation Frequency (Hz)
(B1)
tMTF
Vector Strength
P14 WT
P14 KO
Modulation Frequency (Hz)
(B2)
tMTF
P21 WT
P21 KO
Modulation Frequency (Hz)
(B3)
tMTF
P34 WT
P34 KO
Modulation Frequency (Hz)

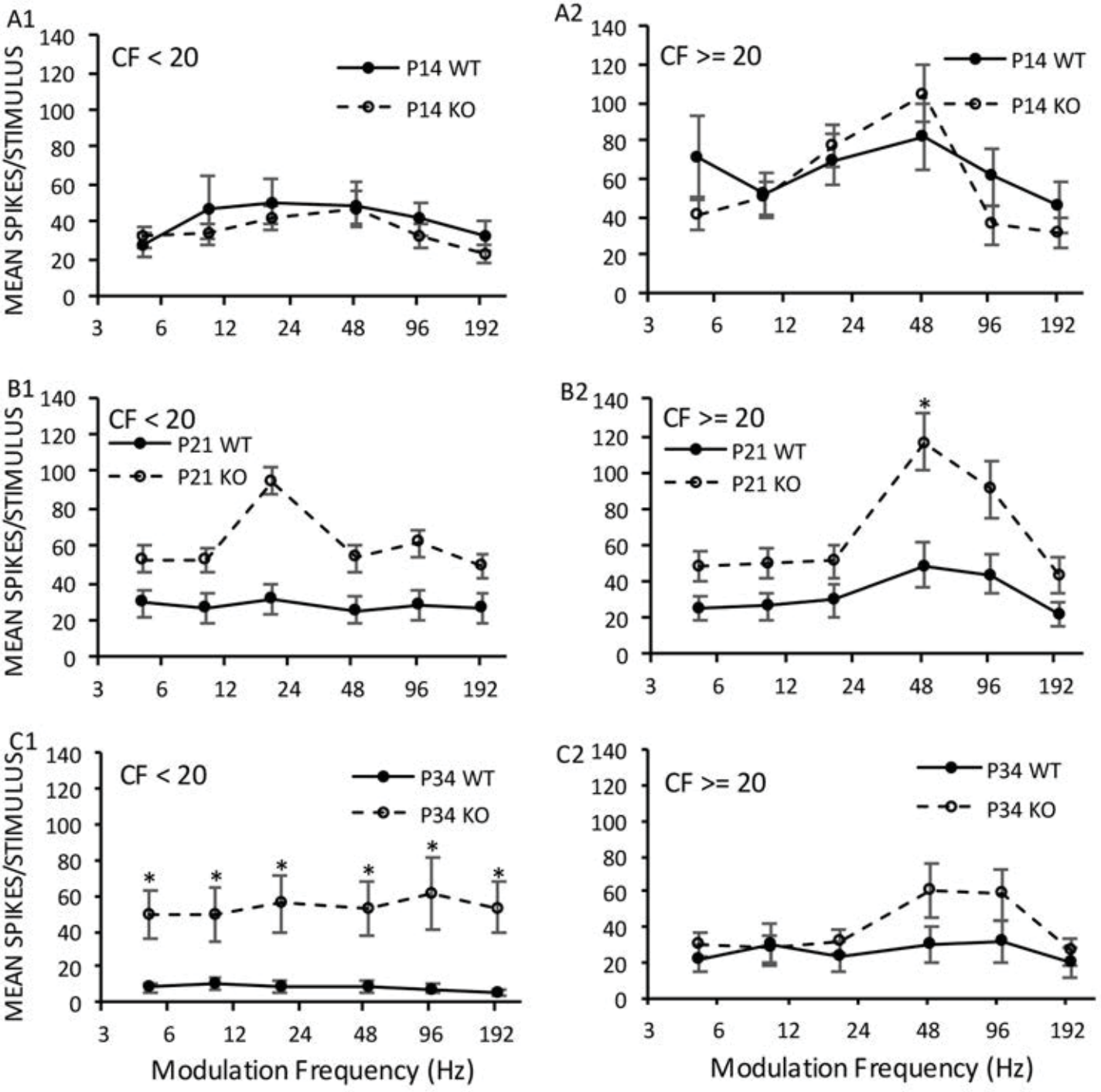
A1
CF < 20
P14 WT
P14 KO
MEAN SPIKES/STIMULUS
A2
CF >= 20
P14 WT
P14 KO
B1
CF < 20
P21 WT
P21 KO
MEAN SPIKES/STIMULUS
B2
CF >= 20
P21 WT
P21 KO
C1
CF < 20
P34 WT
P34 KO
MEAN SPIKES/STIMULUS
Modulation Frequency (Hz)
C2
CF >= 20
P34 WT
P34 KO
Modulation Frequency (Hz)

FIGURE 10

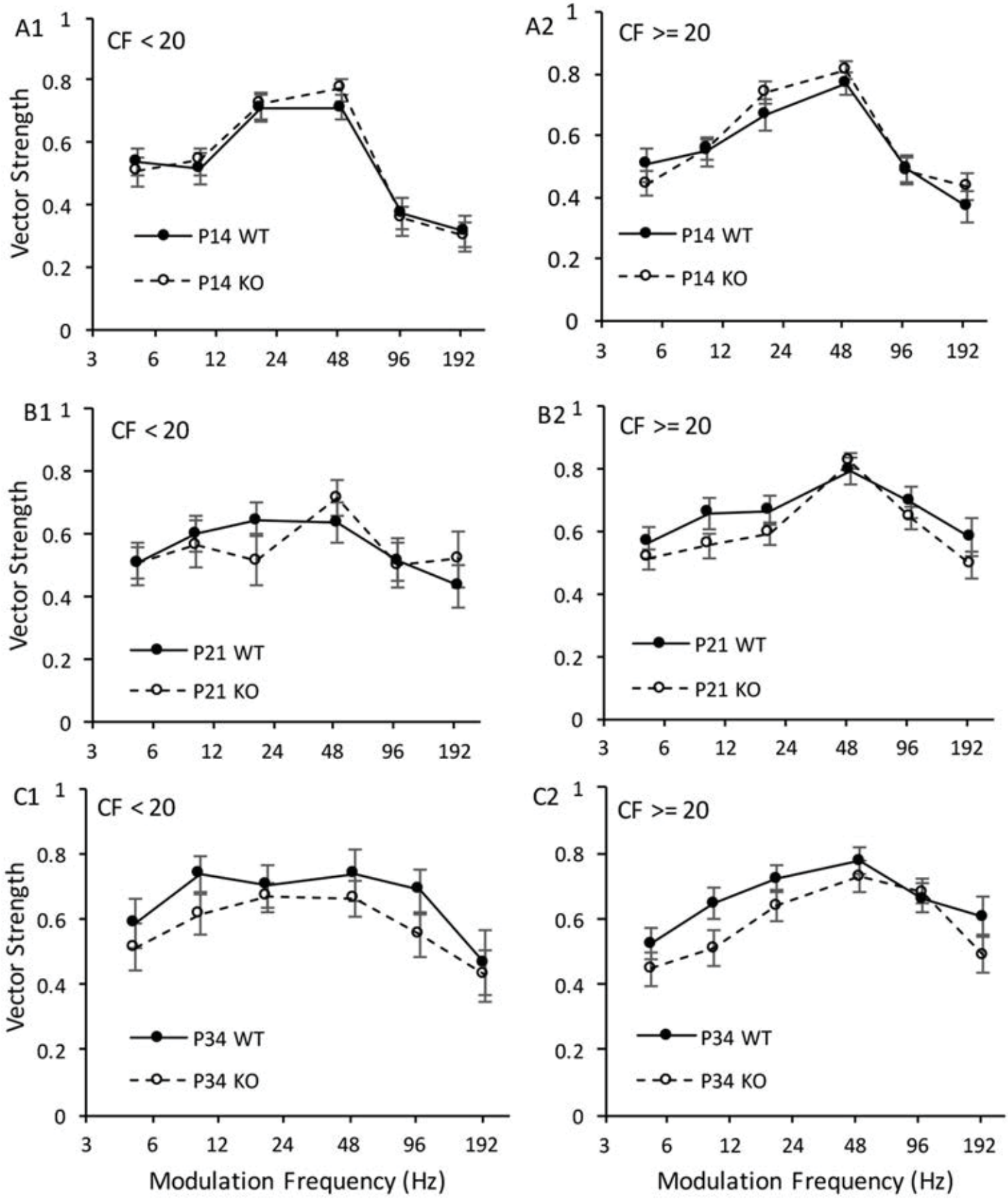
A1
CF < 20
A2
CF >= 20
B1
CF < 20
B2
CF >= 20
C1
CF < 20
C2
CF >= 20
Vector Strength
P14 WT
P14 KO
P21 WT
P21 KO
P34 WT
P34 KO
0
0.2
0.4
0.6
0.8
1
3
6
12
24
48
96
192
Modulation Frequency (Hz)

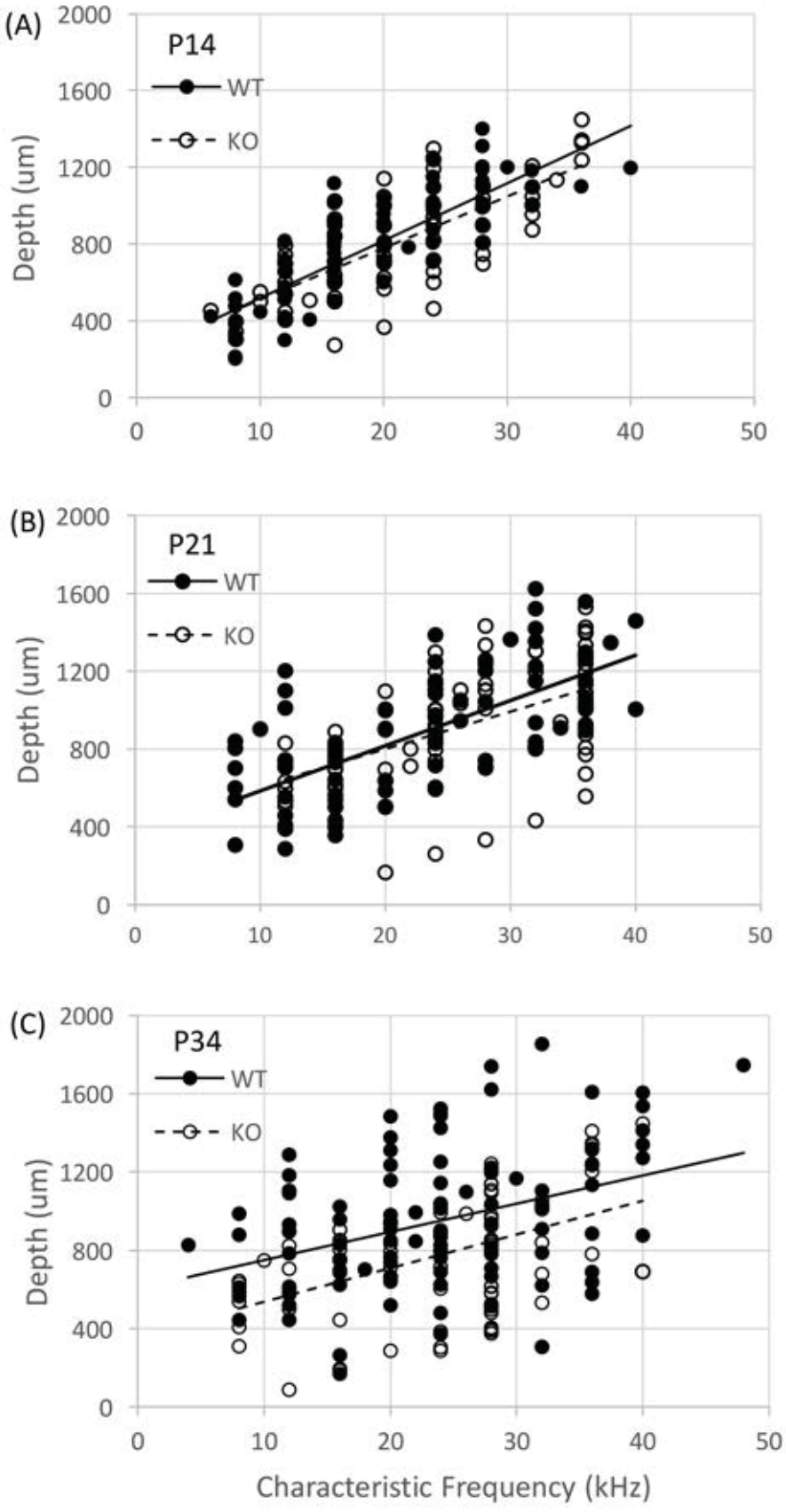
(A)
P14
WT
KO
Depth (um)
2000
1600
1200
800
400
0
0
10
20
30
40
50
(B)
P21
WT
KO
Depth (um)
2000
1600
1200
800
400
0
0
10
20
30
40
50
(C)
P34
WT
KO
Depth (um)
2000
1600
1200
800
400
0
0
10
20
30
40
50
Characteristic Frequency (kHz)